Orchestration of immune function through STIM1-modulated calcium signaling in murine microglia

Hye Min Lim

Department of Medical Science

The Graduate School, Yonsei University

Orchestration of immune function through STIM1-modulated calcium signaling in murine microglia

Directed by Professor Joo Young Kim

The Doctoral Dissertation
submitted to the Department of Medical Science,
The Graduate School of Yonsei University
in partial fulfillment of the requirements for the degree of
Doctor of Philosophy

Hye Min Lim

December 2015

This certifies that the Doctoral

Dissertation of Hye Min Lim is approved.

_____

Thesis Supervisor: Joo Young Kim

_____

Thesis Committee Member #1: Jae Jin Song

_____

Thesis Committee Member #2: Hyoung-Pyo Kim

_____

Thesis Committee Member #3: Seok Jun Moon

_____

Thesis Committee Member #4: Je Wook Yu

The Graduate School

Yonsei University

December 2015

TABLE OF CONTENTS

LIST OF FIGURES

ABSTRACT

Orchestration of immune function through STIM1-modulated calcium signaling in murine microglia

Hye Min Lim

Department of Medical Science
The Graduate School, Yonsei University

(Directed by Professor Joo Young Kim)

It is well established that the differentiation of microglia into active immune cells is governed by increase of sustained intracellular Ca^{2+} concentration ($[Ca^{2+}]_i$) in the cytoplasm, which is maintained by SOCE (store-operated calcium entry). Acute movements of immune cells are also controlled by Ca^{2+} signaling, especially by changes in the Ca^{2+} concentration within micro-domains ($[Ca^{2+}]_{micro\text{-}domains}$) at the cell periphery. The role of STIM1 in chronic and global $[Ca^{2+}]_i$ changes, which governs the proliferation, gene expression and differentiation into active immune cells, has been well examined. However, the role of STIM1 in regulating peripheral $[Ca^{2+}]_{micro\text{-}domains}$ in immune cells, including microglia, has not been studied yet. In this study, we found that murine *Stim1^-/-* microglia showed severe defects in their acute movements, including purinergic stimulation-induced phagocytosis and chemotaxis, which is controlled by Ca^{2+} signaling in $[Ca^{2+}]_{micro\text{-}domains}$. Interestingly, *Stim1^-/-* microglia exhibited highly fluctuating local $[Ca^{2+}]_{micro\text{-}domains}$ changes at the cell periphery, and these fluctuations disappeared completely once mitochondrial membrane potential disruptors were added. *Stim1^-/-* microglia also show attenuated movements of Oria1 upon amoeboid shape-change induced by LPS, which seems to

be related to the partial reduction in $[Ca^{2+}]_{micro-domains}$ fluctuations achieved by SOCE inhibitors. Our new discovery indicates that STIM1 is a critical controller of the local $[Ca^{2+}]_{micro-domains}$, not only through its regulation of SOCE pores, but also through its coordination of mitochondrial Ca^{2+} buffering capacity in micro-domains of the cell periphery

In conclusion, STIM1 is a fundamental regulator of the Ca^{2+} signaling that is required for proper immune functioning of microglia. In that process, in addition to regulating sustained $[Ca^{2+}]_i$ changes, STIM1 also controls $[Ca^{2+}]_{micro-domains}$ changes through coordinating mitochondrial Ca^{2+} buffering capacity *via* local SOCE pores.

Orchestration of immune function through STIM1-modulated calcium signaling in murine microglia

Hye Min Lim

Department of Medical Science

The Graduate School, Yonsei University

(Directed by Professor Joo Young Kim)
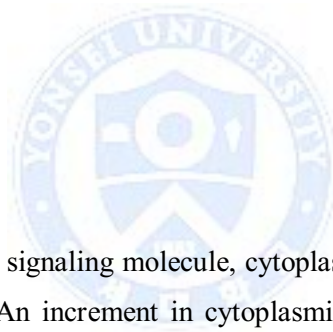
I. INTRODUCTION

As an intracellular signaling molecule, cytoplasmic Ca^{2+} is one of the most widespread and versatile. An increment in cytoplasmic Ca^{2+} levels triggers many processes, and supports various actions of immune cells.[1,2] Cytoplasmic Ca^{2+} increases following Ca^{2+} release from intracellular organelles and from Ca^{2+} influx across the plasma membrane.[3] Ca^{2+} signaling is essential for microglial function, however this has not been completely investigated.[4] Ca^{2+} influx through store-operated calcium entry (SOCE), mediates sustained Ca^{2+} increase during the activation of immune functions in microglia.[5,6] The concept of SOCE was first suggested by James Putney's 'capacitative Ca^{2+} entry' hypothesis.[7]

The discovery of two central molecular components of SOCE, STIM1 and ORAI1, has allowed genetic and molecular manipulation of the SOCE pathway.[8] The internal Ca^{2+} store has a limited capacity, and Ca^{2+} release from internal stores is transient. So, Ca^{2+} entry from the extracellular environment following an initial transient Ca^{2+} release, is an indispensable process for many cellular functions.[9]

3

STIM1 and STIM2 have been identified over the past few years. Together, they constitute the only known protein family that function simultaneously as internal Ca^{2+} storage sensors, and as regulators of Ca^{2+} influx from the extracellular environment. STIM1 is a Type 1, single-spanning transmembrane protein containing an EF-hand Ca^{2+}-binding motif, which functions as a sensor of Ca^{2+} levels in the lumen of the endoplasmic reticulum (ER). Depletion of ER-luminal Ca^{2+} stores induces a conformational change in STIM1. Binding of the C-terminal transmembrane domain of STIM1 activates the plasma membrane store-operated channel leading to Ca^{2+} influx.[2,10-14] STIM2 is a homolog of STIM1, and it shares many features. It is reported that STIM2 contains an EF hand Ca^{2+}-binding motif with a lower affinity for Ca^{2+} than that of STIM1, and that it maintains basal Ca^{2+} concentration in various cells.[5,15] ORAI1 has four transmembrane domains (TM1–TM4) in the plasma membrane. Both its N-terminus and C-terminus face into the cytoplasm. ORAI1 is a selective, Ca^{2+} channel used to elevate cytosolic Ca^{2+} levels rapidly.[2,3] ORAI1, also known as CRAC (Ca^{2+} release-activated Ca^{2+} Channel), is fundamental to immune cell functioning and it has a vital role in the normal physiology of many other cell types.[5,6,8,16-22]

Microglia are specialized macrophages found in the central nervous system (CNS). They are of hematopoietic origin, acting as primary responding cells during infection and tissue injury.[23-26] Lipopolysaccharide (LPS), which is an agonist of Toll-like receptor 4 (TLR4), is widely used to enhance microglial activation and to accelerate several morphological changes. These include phagocytosis and secretion of pro-inflammatory mediators,[18,23,27-31] which are both dependent on a sustained increase in the intracellular Ca^{2+} concentration ($[Ca^{2+}]_i$).[23,28] LPS also induces a shift in the microglial gene expression profile, which is mainly mediated by the NFAT transcription factor.[32] LPS-stimulation leads to a chronic elevation of basal $[Ca^{2+}]_i$ along with a suppression of receptor-evoked calcium signaling.[28] Microglia activated by LPS have increased levels of cytokine secretion; such as TNF-α and IL-6, and show enhanced phagocytic activity.[18] Both UDP-mediated phagocytosis[33] and ATP-induced chemotaxis[41] are regulated primarily by the local $[Ca^{2+}]$ in focal

micro-domains ($[Ca^{2+}]_{micro-domains}$) found at the edge of cells, near the phagosome or focal adhesion spot, for example.[34,35,36]

Meanwhile, there is now a growing awareness that 'local Ca^{2+} signals' or 'Ca^{2+} micro-domains', can be generated by opening Ca^{2+} channels.[37-39] The most fundamental local Ca^{2+} signal is the Ca^{2+} micro-domains that develops rapidly next to open plasmalemmal Ca^{2+} channels; such as voltage-gated L-type ($Ca_v1.2$) and SOCE. Ca^{2+} micro-domains arising from these channels are remarkably versatile in triggering a range of responses that differ enormously in both temporal and spatial profile.[39] It has been anticipated that a regulatory relationship might exist between mitochondria the controlled SOCE of STIM1, since mitochondria can buffer Ca^{2+} within micro-domains by taking up Ca^{2+} *via* mitochondrial Ca^{2+} uniporters working at high $[Ca^{2+}]$.[40-42] The positioning of mitochondria close to ORAI1 channel clusters was reported,[40] and Ca^{2+} buffering by mitochondria was involved in sustaining Ca^{2+} influx through ORAI1 by attenuating the Ca^{2+}-sensitive inactivation of ORA1. On the other hand, *Stim1^{-/-}* mouse embryonic fibroblasts (MEF) showed elongated mitochondria for unknown reason,[43] and mitofusin-2, one of the proteins found on mitochondria that tethers to ER membranes, was required for the mitochondrial membrane potential to exert an effect on the magnitude of SOCE influx.[44] However, the suspected relationship between mitochondria and the controlled SOCE of STIM1 has been neglected since the discovery of the effect of mitofusin-2 on SOCE. Indeed, the working machinery regulating micro-domains Ca^{2+} levels remains completely unrevealed. In this study, we serendipitously discovered retarded motions of ORAI1, remaining at the cell periphery of LPS-stimulated *Stim1^{-/-}* microglia. We also found that they contributed to dramatic fluctuations in the local $[Ca^{2+}]_{micro-domains}$. Notably, the fluctuations completely disappeared following treatment with mitochondrial membrane potential disruptors; and they were partially inhibited by SOCE inhibitors, such as an extracellular ORAI1 antibody (Ex-ORAI1) and the small molecule SKF-96365. Here, we suggest that the migration defects in *Stim1^{-/-}* microglia originated with the fluctuating local $[Ca^{2+}]_{micro-domains}$, which is caused by mitochondrial Ca^{2+} buffering.

Here, we report that STIM1 is an critical controller of the local $[Ca^{2+}]_{\text{micro-domains}}$ that mediates purinergic activated movements of microglia, not only through regulating SOCE pores, but also through coordinating the mitochondrial Ca^{2+} buffering capacity in micro-domains at the cell periphery.

.

II. MATERIALS AND METHODS

1. Generation of *Stim1*^{-/-} mice

Stim1^{+/-} heterozygotic mice (C57BL/6) were generated as previously described.[6] The mice were bred and maintained according to the Yonsei Medical Center animal research requirements, and the Committee on Animal Research at Yonsei Medical Center approved all procedures (protocol number 2011-0112). As *Stim1*^{-/-} mice die within one day of birth, embryos in the 17th day of pregnancy were used for experiments; and these were generated by mating of *Stim1*^{+/-} female mice with *Stim1*^{+/-} male mice. Genomic DNA isolated from the embryo tail was used for genotyping, and was extracted using prepGEM Tissue (PTI0200; ZyGEM, Hamilton, New Zealand).

2. Reagents and solutions

The reagents that Lipopolysaccharide (LPS) from *Escherichia coli* 0111:B4 (L4391), thapsigargin (TG; T9033), uridine 5'-(trihydrogen diphosphate) sodium salt (UDP; U4125), adenosine 5'-triphosphate di(tris) salt hydrate (ATP; A9062); were repetitively used. All reagents were purchased from Sigma. (Sigma Aldrich, St. Louis, MO, USA).

For primary cell cultures, DMEM/F12 (1:1) culture medium (Dulbecco's modified Eagle medium, 11320-033), Fetal bovine serum (FBS) (26140-079), Penicillin-streptomycin (15140-122; Gibco, Life technologies[TM], Carlsbad, CA, USA); Trypsin 0.25% (1x) solution (SH30042.01; Hyclone laboratories, Thermo scientific, Logan, UT, USA) were used. For RT-PCR analysis, TRIzol reagent (Invitrogen, Life technologies[TM], Carlsbad, CA, USA); AccuScript High Fidelity 1st Strand cDNA Synthesis Kit (200436; Agilent Technologies, Santa Clara, CA, USA); Solg[TM] 2x Taq PCR Smart mix (STD02-M10h; SolGent Co., Daejeon, Korea) were used.

For immunoblotting, NaCl (S7653), Triton X-100 (T8787), Glycerol (G5516;

Sigma Aldrich); EDTA (15694, Usb, USB Coporation, Cleveland, OH, USA); Tris Ultrapure (T1501, Duchefa, Haarlem, The Netherlands); Complete proteinase inhibitors (Roche Applied Science, Mannheim, Germany); HCl (084-05425), NaOH (196-05375, Wako, Osaka, Japan); BCA Protein Assay Kit (23227; Pierce™, Thermo Scientific, Rockford, IL, USA); 5x Tricine-SDS sample buffer (KTR020-5), pre-made 4-12% gradient SDS-PAGE gels (KG5012) (KOMA Biotech, Seoul, Korea) were used.

For Ca^{2+} imaging experiments, NaCl (S7653), KCl (P5405), $MgCl_2$ (M8266), Glucose (G6152), HEPES (H3375), $CaCl_2$ (C1016), EGTA (E3889), cyclopiazonic acid (CPA; C1530), SKF-96365 (S7809), Streptomycin (S6501), 2-APB (D9754), CCCP (C2759), Rotenone (R8875; Sigma Aldrich), and Fura-2 AM (F1201; Invitrogen, Molecular probes, Eugene, Oregon, USA) were used.

For phagocytosis, 0.4% Trypan blue stain (15250-061), 0.05% trypsin-EDTA (25300-062, Gibco, Life technologies™, Carlsbad, CA, USA); BioParticles Fluorescent Particles (conjugated with Alexa Fluor 488; E-13231, Invitrogen, Molecular probes, Eugene, Oregon, USA) were used. For Elisa assay, TNF-α (430901), IL-6 (431301) ELISA kit (BioLegend, San Diego, CA, USA) were used. For in vitro and in vivo chemotaxis assay, fibronectin (F0895), methylene blue (66720; Sigma Aldrich) were respectively used.

For immunocytochemistry, 4% Paraformaldehyde (19943), bovine serum albumin (BSA) (10857; Affymetrix, Cleveland, Ohio, USA); Horse serum (16050-122, Gibco); Gelatin (G1890), Sodium azide (S2002), Phosphate-buffered saline (PBS) (P5493, Sigma Aldrich) were used.

3. Antibodies and fluorescent dyes

Anti-Stim1 (610954; BD Transduction Laboratories™ San Jose, CA, USA), anti-Stim2 (4917; Cell Signaling, Danvers, MA, USA), aldolase A (N-15) (sc-12059; Santa Cruz Biotechnology, Santa Cruz, CA, USA), anti-Iba-1 (019-19741; Wako, Osaka, Japan), Ex-Orai1 (ACC-062; Alomone labs, Jerusalem, Israel) and appropriate secondary antibodies; Alexa Fluor-FITC (A11070), Alexa Fluor-

rhodamine (A11004, Invitrogen, Molecular probes, Eugene, Oregon, USA) were used. Dyes for microglia, tomato lectin (conjugated with Dylight 594, Vector Labs, Carlsbad, CA, USA), for nuclei, 4,6-diamidino-2-phenylindole (DAPI; D3571) and for mitochondria, Mito tracker Deep Red FM (M22426, Invitrogen, Molecular probes, Eugene, Oregon, USA). Stained cells on coverslips were mounted with fluorescent mounting medium (S3023, Dako, Glostrup, Denmark).

4. Isolation and culture of primary mouse microglia

Primary cell cultures of microglia were prepared from the whole brain of mice at embryonic day 17 (E17).[45] Each embryo tail was used for genotype analysis. Primary mixed cells were chemically and mechanically dissociated from the whole brain and seeded in DMEM/F12 (1:1) supplemented with 10% FBS and 1% penicillin-streptomycin as described previously.[18] Cells were cultured at 37 °C with 5% CO_2 in an incubator (Thermo Fisher Scientific, Marietta, OH, USA). Confluency was achieved after ~3-4 wk. After 4 wk, primary mixed cells of wild-type (WT), $Stim1^{-/-}$ mice were subject to mild trypsinization by the shaking method.[45,46] The upper cell layer of mixed cells was removed by treatment with a 0.25% (1x) trypsin solution diluted 1:4 in culture medium for 20 min at 37 °C. The medium mixed with trypsin was replaced with 12 ml of fresh culture medium. The pure microglia attached to the bottom of the T75 flask. These cells were isolated by shaking the flasks at 120 rpm (SLOS-20; SeouLin Bioscience, Seoul, Korea) at 37 °C with 5% CO_2 in an incubator for 1 hr and then, all medium of each flask were collected separately. Each flask was refilled with 12 ml of new medium. Next, the collected medium were placed on a cell strainer with a pore size of 40 μm (352340; BD Falcon, San Jose, CA, USA) and were filtered into a fresh 15 ml conical tube. Centrifuge at 2,500 RCF at room temperature for 5 min. Resuspend the cell pellet and the number of cells was then counted using a hemocytometer (Marienfeld, Lauda-Königshofen, Germany).

5. Reverse-transcriptase PCR analysis

Total RNA was extracted with TRIzol reagent according to the manufacturer's instructions. cDNA was synthesised using AccuScript High Fidelity 1st Strand cDNA Synthesis Kit according to the manufacturer's instructions. RT-PCR was performed in triplicate using $Solg^{TM}$ 2x Taq PCR Smart mix. Each RT-PCR reaction contained 100 ng of cDNA. The thermocycling conditions of RT-PCR were an initial denaturation at 95 °C for 5 min followed by 31~37 cycles of 95 °C for 30 sec, 58 °C for 40 sec and 72 °C for 40 sec, and a last extension at 72 °C for 7 min.

The primer sets are provided as follows (S, sense; AS, antisense) were used for PCR analyses for *Stim1*, S, 5'-GGAAGACCTCAATTACCATGAC-3' and AS, 5'-GCTCCTTAGAGTAACGGTTCTG-3' ; for *Stim2*, S, 5'-TGAGGATACCCTGCA GTGG-3' and AS, 5'-CAGTCTGCAGACTCTCTAAGTC-3' ; for *Orai1*, S, 5'-TGTTTGCCCTCATGATCAGCAC-3' and AS, 5'-AAACTCGGCCAGCTCATTG AG-3' ; for *Orai2*, S, 5'-TTGCGATTTGCTACCAACCTG-3' and AS, 5'-GCTGGCTTTGGGAATTCACC-3' ; for *Orai3*, S, 5'-TGCAAGCATTGCCTCAG AAAC-3' and AS, 5'-GGATGCCAACTGCAAAGCAG-3'.

To confirm the mRNA expression of P2 receptors, RT-PCR primer set for P_2X_4, S, 5'-ATGGCAGGCTGCTGCTCCGT-3', and AS, 5'-AGCTGGCGTTGGCACAC CA-3' ; for P_2X_7, S, 5'-ATGCCGGCTTGCTGCAGCT-3' and AS, 5'-TCGGCGCT CCTCAAGAGTG-3' ; for P_2Y_6, S, 5'- ATGGAGCAGGACAATGGCACC-3' and AS, 5'-ACACAGTGCGGTTGCGCTG-3' ; for P_2Y_{12}, S, 5'-ATGGATGTGCCTGG TGTCAACACC-3' and AS, 5'-CGTGCCAAACTAGACCAAACTCTGAC-3' were used. *Actin* primers sets for S, 5'-GACCCAGATCATGTTTGAGACC-3' and AS, 5'-GGCCATCTCCTGCTCGAAGTC-3' were used as loading control. *GFAP* primers sets for S, 5'-TGATGGAGCTCAATGACCG-3' and AS, 5'-CATCTGCCT CCTGTCTATACGC-3' were used as negative control.

To confirm the mRNA expression of SACCs, RT-PCR primer set for *Trpv1*, S, 5'-GATGACTTCCGGTGGTGCTTCAGG-3', and AS, 5'- CTGGGTGCTATGCCT ATCTCGAGTG-3' ; for *Trpv2*, S, 5'- GGGAGGCTGCTGAAAGTTGGC-3', and AS, 5'-TGGTCTTCCTCTGAGGCACTGTTC-3' ; for *Trpv4*, S, 5'-AACAAGAG

ATGGAGGAGAAAGGTCG-3', and AS, 5'-CTCATCAGTCAGGCGCTTCTTGT GG-3' ; for *Trpm3*, S, 5'- GGGCTTACCGCTGCAACTACACG-3', and AS, 5'-CGGCCCACACCATCAGCTC-3' ; for *Trpm7*, S, 5'-TCCCGACAATCTGTGGT CCTGG-3', and AS, 5'-GATAAGAGGAGGAGGCAGGACTGG-3' ; for *Trpp2*, S, 5'- CAAGTACTGGTGAGGCGCGTGGAC-3', and AS, 5'- CTGCTCCCTGTGG ATCTCACTGTC-3'. *18srRNA* primers sets for S, 5'-GTGGAGCGATTTGTCTGG TT-3' and AS, 5'-CGCTGAGCCAGTCAGTGTAG-3' were used as loading control.

To confirm the mRNA expression of IP$_3$R and Ryanodine (Ryr) receptors in ER , RT-PCR primer set for *IP$_3$R1*, S, 5'-TGTTTGCTGCAAGGGTGATCTACG-3', and AS, 5'-TCCTTCACTTTCACCAGCACGATG-3' ; for *IP$_3$R2*, S, 5'-ATTGTCA CCGTGCTGAACCAGG-3', and AS, 5'-TCACTTCTGAGGTCAGCAAACGTG-3' ; for *IP$_3$R3*, S, 5'-AGAAGAGGACGAGGAGCCCGATAG-3', and AS, 5'-TCTCCAGACCACAGATGAAGCACG-3' ; for *Ryr1*, S, 5'- GGCTGGTACATGG TGATGTCCCTC-3', and AS, 5'- GAATTTGCGGAAGAAGTTGAAGGC-3' ; for *Ryr2*, S, 5'- TGAGTTACTGGGCATGGATAAGGC-3', and AS, 5'- CGATGTCAA GGAGGTGAGCAGC -3' ; for *Ryr3*, S, 5'- GAGGCAGCATCTCTGGTGTCATG - 3', and AS, 5'-CCTCAAGGTCTTAAAGCCCATTGC-3', and the mRNA expression of SERCA, RT-PCR primer set for *Serca1* (*Atp2a1*), S, 5'-ATCTTCAAGCTCCGGGCCCT-3', and AS, 5'-CAGCTTTGGCTGAAGATGCA-3' ; for *Serca2* (*Atp2a2*), S, 5'-CTGTGGAGACCCTTGGTTGT-3', and AS, 5'-CAGAGCACAGATGGTGGCTA-3'.

To confirm the mRNA expression of mitochondrial Ca^{2+} transporters, RT-PCR primer set for *Mcu*, S, 5'-GTGGGAGCCGCATATTGCAGTAC-3', and AS, 5'-CCGATCCTCCTCTTGCAGTTGTC-3' ; for *Ncx1 (Slc8a1),* S, 5'- GGAGCTGGC AACATCTTGAAGAGG-3', and AS, 5'-CAAACACAGTGGTGCTCAAGTCGC-3' ; for *Letm1*, S, 5'-GGTTGACGAGCCGTGAGAGTGTTC-3', and AS, 5'-CGCCCTCCTCCAGCTTCTTATTC-3' ; for *Vdac1*, S, 5'-CCTCCCACATACGCC GATCTTG-3', and AS, 5'-ACGTCAGCCCATACTCAGTCCATC-3' ; for *Vdac2*, S, 5'-CGATGTGTATCCCTCCACCCTATG-3', and AS, 5'-CCCAGAGTGTTATCGG TGTTCCAC-3' ; for *Vdac3*, S, 5'-GGTTGGCTTGCTGGCTATCAGATG-3', and

AS, 5'-TGTTGTTGCTGCCAGCTGTCC-3'.

To confirm the mRNA expression of mitochondrial tether genes, RT-PCR primer set for *Mitofusin-1*, S, 5'-GAAAGCCATCACTGCAATCTTCGG-3', and AS, 5'- AAATGCCACCTTCATATGTCTCCG-3'; for *Mitofusin-2*, S, 5'- GAGCA ATGGGAAGAGCACCGTG-3', and AS, 5'-GCATGGGCCAGTTGGTTCACAG-3'; for *Miro-1* (*Rhot1*), S, 5'-TCGCTGGTCAGTGAAGAATTTCCG-3', and AS, 5'-AGAGGAATCCATCGGCTTGTTACC-3'; for *Miro-2* (*Rhot1*), S, 5'-ACGTCT CTGATCCTGTCGCTGGTC-3', and AS, 5'-TGGTGGTCTCCTCAGACACATCG -3'. RT-PCR results were quantified by calculating the band intensity using Multi Gauge software (Fuji Film).

6. Immunoblotting

Immunoblotting was performed as described previously.[47] Primary cultured WT and *Stim1*^{-/-} microglia were seeded into 6-well plates at 2 x 10^6 cells/well and incubated overnight at 37 °C with 5% CO_2 atmosphere. Then, cells were lysed in lysis buffer [150 mM NaCl, 5 mM Na-EDTA, 10% glycerol, 20 mM Tris-HCl, pH 8.0, 0.5% Triton X-100, and complete protease inhibitors]. Protein concentration was quantified using a colorimetric method (BCA Protein Assay) according to the manufacturer's instructions. The lysates, which contained 40 µg of protein, were eluted with 5x Tricine-SDS sample buffer, and the eluted lysates were separated on pre-made 4-12% gradient SDS-PAGE gels. Primary antibodies included anti-Stim1, anti-Stim2, and aldolase A (N-15). Appropriate secondary antibodies were used.

7. Single live cell [Ca^{2+}]$_i$ imaging

Single live cell [Ca^{2+}]$_i$ imaging was performed by recording [Ca^{2+}]$_i$ using Fura-2 AM labeling at dual excitation wavelengths of 340/380 nm, ratiometrically, as described previously.[18] Briefly, WT and *Stim1*^{-/-} microglia 5-10 x 10^3 cells were plated in the middle of 18 mm ø cover glass (Paul Marienfeld GmbH, Lauda-Königshofen, Germany) and 3 hr after plating, cells were treated with or without 100 ng/ml LPS for 90 min. After 60 min of LPS-stimulation, cell-permeable 2 µM

Fura-2 AM and incubated for 30 min with the cells at 37 °C with 5% CO_2 in an incubator. Trapped Fura-2 fluorescence was measured with a spectrofluorometer (Photon Technology International, Birmingham, NJ, USA). Cells were perfused with a solution containing 150 mM NaCl, 5 mM KCl, 1 mM $MgCl_2$, 10 mM glucose, 10 mM HEPES (pH 7.4, adjusted with NaOH); containing either 1–2 mM $CaCl_2$ or 5 mM EGTA (to chelate any Ca^{2+} in the solution). The osmolality of all solutions was adjusted to 310 Osm with 2 M NaCl. The Fura-2 ratio was recorded using dual-excitation wavelengths of 340 and 380 nm, and emission wavelengths above 510 nm were monitored. Cells were treated with 25 μM cyclopiazonic acid (CPA), which inhibits the sarco/endoplasmic reticulum Ca^{2+}-ATPase. Cells were treated with either 100 μM UDP or 50 μM ATP and then each single whole cell boundary was drawn for assessment of intracellular Ca^{2+} concentrations $[Ca^{2+}]_i$) during analysis.

A live cell Ca^{2+} imaging system was used to compare the local and short-lived high $[Ca^{2+}]$ micro-domains in cell periphery ('local $[Ca^{2+}]_{micro-domains}$') of WT and $Stim1^{-/-}$ microglia flowing stimulation with either 50 μM ATP or 100 μM UDP. After stimulation, changes in the peripheral $[Ca^{2+}]_{micro-domains}$ ($\sum\Delta F$) were summed over 27 consecutive images acquired at 8 sec intervals among 108 consecutive images; The overlaid regions of color signify the $[Ca^{2+}]_{micro-domains}$ in each microglial cell. The yellow box refers to (Fig. 7A, C) the period of $\sum\Delta F$ calculation during 260–370 sec after ATP-stimulation or during 250–360 sec after UDP-stimulation (Fig. 7B, D).

To check whether the local function of ORAI1 was uncontrolled in $Stim1^{-/-}$ microglia, the changes of peripheral $[Ca^{2+}]_{micro-domains}$ of $Stim1^{-/-}$ microglia were tested in the extreme condition.; 100 ng/ml LPS for 90 min to induce cell rounding, followed by stimulated with 100 μM UDP for 1 min to induce store depletion. The global change of $[Ca^{2+}]_i$ (thick black line in trace) in whole cell (white dotted lines in ratio images, Fig. 8) was measured. Regions of interest (ROIs) in the in cell periphery were colored (red, green, pale blue and purple) in the ratio images, and the matching color curves show the changes in the peripheral $[Ca^{2+}]_{micro-domains}$ within corresponding regions. The height of the yellow box indicates the spatial

13

Ca^{2+} movement and the width of yellow box indicates the period of $\sum\Delta F$ calculation during 530–750 sec after UDP-stimulation in each microglia. The $\sum\Delta F$ were summed over 27 consecutive images acquired at 8 sec intervals among 108 consecutive images (Fig. 8, the ratio of 340/380 nm images (left) and the combined images ($\sum\Delta F$, right).

After 100 ng/ml LPS-stimulation of *Stim1*$^{-/-}$ microglia for 90 min, with 5 μg/ml Ex-Orai1 antibody - which bind to extracellular loop of Orai1 (Fig. 10B) - or without such stimulation (mock cells; treated 1% BSA, 0.05% sodium azide in PBS); the cells were pre-incubated for 10 min at 37 °C with 5% CO$_2$ in an incubator. And then the cells were stimulated by 100 μM UDP for 1 min with solution containing 2 mM Ca^{2+}.

Pharmacological inhibitors used to inhibit the fluctuation included; SKF-96365 (SOC inhibitor), Streptomycin (SACC blocker), 2-APB (IP$_3$R inhibitor), CCCP (protonophore) or Rotenone (Complex I inhibitor for disrupting mitochondrial function). After 100 ng/ml LPS-stimulation of *Stim1*$^{-/-}$ microglia for 90 min, the cell thoroughly washed with solutions containing 2 mM Ca^{2+}, prior to stimulation with 100 μM UDP for 1 min to induce store depletion. Shortly afterwards, cells were treated with 20 μM SKF-96365 (Fig. 10C), 200 μM Streptomycin (Fig. 10A), 100 μM 2-APB (Fig. 9C), 0.5 μM CCCP (Fig. 9D) or 10 μM Rotenone (Fig. 9E) in solutions containing 2 mM Ca^{2+} for 8 min. The $\sum\Delta F$ were summed over 27 consecutive images acquired at 8 sec intervals among 108 consecutive images (Fig. 8-10), differential interference contrast [DIC] and the ratio of 340/380 nm images (left) and the combined images ($\sum\Delta F$, right). The yellow box indicates that the period of $\sum\Delta F$ calculation during 530–750 sec after treatment of the pharmacological inhibitors.

8. Phagocytosis assay

WT and *Stim1*$^{-/-}$ microglia were seeded into 12-well plates at 3 x 10^5 cells/well and incubated at 37 °C overnight. Then, cells were treated with or without 100 ng/ml LPS and incubated for 24 hr at 37 °C with 5% CO$_2$ in an incubator. These

LPS-activated microglia were treated with BioParticles and incubated for a further 2 hr. The cells were then rinsed three times with PBS. To quench the particle fluorescence, cells were stained with 0.4% trypan blue at room temperature (RT) for 2 min, and then cells were rinsed a further three times with PBS. Cells were fixed with 4% paraformaldehyde in PBS at RT for 10 min, and then rinsed three times with PBS. Nuclei were stained with 5 μg/ml DAPI. Cells were visualized on an inverted fluorescence microscope (IX73-F22PH, Olympus) with an excitation wavelength of 488 nm and emission wavelength of 520. Fluorescence intensity was quantified using *MetaMorph* software (Molecular Devices, Sunnyvale, CA, USA). Flow cytometry experiments were conducted as follows. WT and *Stim1*^{-/-} microglia were seeded into 12-well plates at 3×10^5 cells/well and incubated at 37 °C overnight. Then, cells were treated with or without 100 μM UDP and incubated at 37 °C with 5% CO_2 in an incubator for 20, 40 min. UDP-activated microglia were treated with BioParticles as described above. Cells were rinsed three times with PBS, and then to quench the BioParticles, cells were stained with 0.4% trypan blue at RT for 2 min, followed by rinsing three times with PBS. After treatment with 0.05 % trypsin-EDTA at 37 °C for 10 min in 5% CO_2 atmosphere incubator, the cells were harvested by centrifugation at 2,000 rpm at 4 °C for 5 min. Supernatant was removed, 500 *μl* ice-cold serum-free DMEM/F12 (1:1) medium was added, and cells were resuspended. Cells were held on ice and analyzed by flow cytometry using a BD FACSVerse (BD Biosciences, Franklin Lakes, NJ, USA), and a total gated cell number of 10,000 cells. Flow cytometry data were analyzed using *FlowJo* software (Treestar, Ashland, OR, USA).

9. ELISA assay

WT and *Stim1*^{-/-} microglia were seeded into 6-well plates at 2×10^6 cells/well and incubated at 37 °C overnight. Cells were then treated with or without 100 ng/ml LPS and incubated for 24 hr at 37 °C with 5% CO_2 in an incubator. The next day, supernatants were assayed for levels of TNF-α and IL-6 using an ELISA kit according to the manufacturer's instructions. Cytokine levels in LPS-activated

microglia were kinetically analyzed for 30 min (at 5 min intervals) using a VersaMax spectrophotometer plate reader (Molecular Devices, Sunnyvale, CA, USA) at 650 nm.

10. *In vitro* chemotaxis assay

Analysis of microglial migration was performed in triplicate using chemotaxis chambers (101-8, Neuro Probe, Gaithersburg, MD, USA) as previously described.[48-52] Polycarbonate filters with 8 μm pores were coated with 10 μg/ml fibronectin in PBS at RT for 1 h. The lower chambers were filled with 29 *μl* of serum-free DMEM-F12 media containing 50 μM ATP. The dry fibronectin-coated filter was installed to separate the lower chambers from the upper chambers. Then, WT and *Stim1⁻ᐟ⁻* microglia were seeded into the upper chambers at 4 x 10^4 cells/well in 20 *μl* serum-free DMEM-F12, and the chambers were incubated at 37 °C with 5% CO_2 in an incubator for either 15, 30, 60, or 90 min. After incubation, the chemotaxis chambers were disassembled and filters were removed. Microglial in the lower chambers were stained with tomato lectin (1:1000), nuclei were stained with 5 μg/ml DAPI at RT for 10 min, and then cells were rinsed three times with PBS. Cells that had migrated to the lower chambers were visualized and counted using an inverted fluorescent microscope (IX73-F22PH, Olympus, Tokyo, Japan). The total number of cells stained with DAPI was quantified using *MetaMorph* software.

11. Microinjection of embryonic mouse brains *in vivo* and immunohistochemistry.

We used microinjection to target specific regions of embryonic mouse brain *in vivo* as previously described.[53] A microinjector (Nanoliter 2,000) and capillary glass (3.5 inches) (WPI, Sarasota, FL, USA) were used as injection tools. Timed pregnant *Stim1⁺ᐟ⁻* heterozygotic female mice carrying embryonic day 17 (E17) embryos were anesthetized with isoflurane and placed on a heating pad. Embryonic mice *in utero* were injected with 30 *nl* of LPS mixed with 4% methylene blue. The final

concentration was 12 ng of LPS per one embryo *in utero*. The mother was sutured and recovered on a warming pad for 1 h, and then moved back to her home cage. After 24 hr, the mother was re-anesthetized with isoflurane and the abdominal incision was reopened to approach the embryos. After the embryos were taken out of the uterus, the mother was necessarily sacrificed. Embryonic whole brains were fixed with 10% formalin at 4 °C overnight. Then, tissue was transferred to 3 M sucrose in PBS solution and incubated at 4 °C until the tissue sank to the bottom of the tube (a couple of hours). This sucrose-infiltration is necessary for tissue cryopreservation. The fixed embryo brain tissue was used for cryosectioning, and embryo tails were used for genotype analyses. Sections of embryonic WT and *Stim1*^{-/-} brains were labeled in blocking solution with anti-Iba-1, an antibody specific for microglia, and a secondary antibody labeled with Alexa Fluor 488, followed by rinsing three times with PBS. Nuclei were stained with 5 μg/ml DAPI. After rinsing, coverslips were mounted using fluorescent mounting medium and visualized under a confocal microscope (LSM 710 controlled with *Zen* software, Carl Zeiss, Jena, Germany). The total number of cells in lesioned and counterpart areas was measured by computer vision using *MetaMorph* software. More than 3 ea of WT and *Stim1*^{-/-} embryonic mice were analyzed. The relative morphological responses were measured by the average shape factor using computer vision and *MetaMorph* software. The shape factor, defined as 4 A/P^2 (A and P are the cell area and perimeter, respectively), approaches unity for round shaped cells.

12. Immunocytochemistry

Primary cultured WT and *Stim1*^{-/-} microglia were seeded on glass cover slips placed into 24-well plates at 5 x 10^4 cells/well, and incubated overnight at 37 °C with 5% CO_2 in an incubator. Cells were treated with or without 1 μM TG for 5 min, 100 μM UDP for 40 min or 100 ng/ml LPS for 90 min, before being fixed with 4% paraformaldehyde in PBS at RT for 10 min, followed by rinsing three times with PBS. To avoid non-specific antibody binding, cells were treated with blocking solution [5% horse serum, 1% BSA, 0.1% gelatin, 0.001% sodium azide in PBS, pH

7.4] at RT for 30 min. To detect functional ORAI1 at the cell surface, an antibody recognizing the extracellular loop of Orai1 (Ex-Orai1) was used under non-permeabilizing conditions, which prevented antibody penetration into cells. After Ex-Orai1 labeling with primary and secondary antibodies, cells were permeabilized and STIM1 was labeled. Cells were permeabilized by incubating in permeabilization solution [0.1% Triton X-100, 1% horse serum, 1% BSA in PBS, pH7.4] at RT for 5 min, and were then rinsed three times with PBS. Immunostaining was performed in blocking solution using 1:100 dilution Ex-Orai1 or 1:100 dilution of anti-Stim1 as primary antibodies, followed by the appropriate secondary antibodies tagged with Alexa Fluor-FITC (1:200) or Alexa Fluor-rhodamine (1:200). Nuclei were stained with 5 μg/ml DAPI. The coverslips were rinsed, mounted with fluorescent mounting medium, and cells were visualized on a confocal microscope.

For mitochondrial staining, primary cultured WT and $Stim1^{-/-}$ microglia were seeded on glass cover slips into 24-well plates at 5×10^4 cells/well and incubated overnight at 37 °C with 5% CO_2 in an incubator. Cells were treated with or without 100 ng/ml LPS for 90 min and were stained with 200 nM Mito Tracker in culture medium for 10 min at 37 °C in an incubator, and nuclei were stained with 5 μg/ml DAPI. Following staining, cells were fixed with 4% paraformaldehyde in PBS at RT for 5 min and mounted with fluorescent mounting medium.
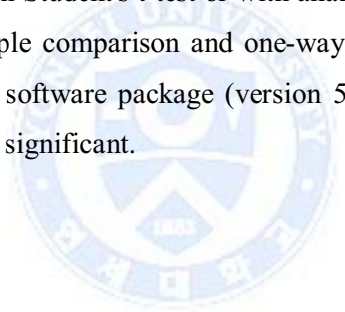
13. Transmission Electron microscopy

Each 1×10^5 cells/well of WT and $Stim1^{-/-}$ microglia were seeded on 12 mm diameter inserts of transwell plate (Corning, 3460, USA) with or without LPS, and incubated for 90 min at 37 °C with 5% CO_2 in an incubator. Cells were centrifuged and the supernatant was removed. The pellets were resuspended and fixed with solution [2% Glutaraldehyde - Paraformaldehyde in 0.1 M phosphate buffer (PB) (pH 7.4)] for 12 hr, and washed out with 0.1 M PB. Cells were post-fixed with 1% OsO4 dissolved in 0.1 M PB for 2 hr and dehydrated in ascending gradual series (50~100%) of ethanol and infiltrated with propylene oxide. Specimens were embedded by Poly/Bed 812 kit (Polysciences). After fresh resin embedding and

polymerization at 65℃ electron microscope oven (TD-700, DOSAKA, Japan) for 24 hr. Thick section of about 200–250 nm was firstly cut and stained with *toluidine blue* (sigma, T3260) for light microscope. Thin section of about 80–100 nm were double stained with 6% *uranyl acetate* (EMS, 22400 for 20 min) and *lead citrate* (Fisher, for 10 min) for contrast staining. These sections were cut by LEICA EM UC-7 (Leica Microsystems, Austria) with a diamond knife (Diatome) and transferred on copper grids. The images of thin section were visualized using camera-Megaview III (Soft imaging system-Germany).

14. Statistical analysis

Data are presented as the means ± standard error of the mean. Statistical analysis was performed with Student's t-test or with analysis of variance (ANOVA), followed by Tukey's multiple comparison and one-way or two-way ANOVA tests using the GraphPad Prism software package (version 5.0), as appropriate. $P<0.05$ was considered statistically significant.

III. RESULTS

1. Validation of the expression of SOCE components and their function in primary cultured WT and *Stim1*^{-/-} microglia

Both ORAI and STIM proteins are major components of the SOCE system. We tested the mRNA expression of each isoform of *Orai-* (*Orai1*, *Orai2*, and *Orai3*) and *Stim-* (*Stim1* and *Stim2*) families in C57BL/6 strain WT and *Stim1*^{-/-} primary cultured microglia using RT-PCR analysis, checking for any alterations in gene expression. The purity of microglial cDNA was confirmed by GFAP-negative results; *β*-actin was used as control for cDNA loading. *Orai1*, *Orai2*, and *Orai3*, and *Stim2* were expressed in both microglial cell types (Fig. 1A). *Stim1*^{-/-} microglia did not contain *Stim1* transcripts, and had slightly elevated *Orai2* expression.

In addition, the expression of STIM1 and STIM2 expressions was analyzed by measuring LPS-induced protein levels (Fig. 1B). Production of STIM1 protein was increased by LPS treatment in WT, while STIM2 was slightly increased. These results testify that STIM1 is the primary SOCE regulator in microglia.

The Ca^{2+} influx induced by internal Ca^{2+} store depletion was compared to basal $[Ca^{2+}]_i$ levels by measuring Fura-2 AM loading inside microglia. These cells had been treated with CPA, which inhibits SERCA; the sarco/endoplasmic reticulum Ca^{2+} ATPase (Fig. 1C-F). Relative to WT cells, *Stim1*^{-/-} microglia had a reduced basal $[Ca^{2+}]_i$, reduced internal Ca^{2+} store, and Ca^{2+} influx was essentially blocked. These data demonstrate that STIM1 is a major regulator of SOCE in microglia.
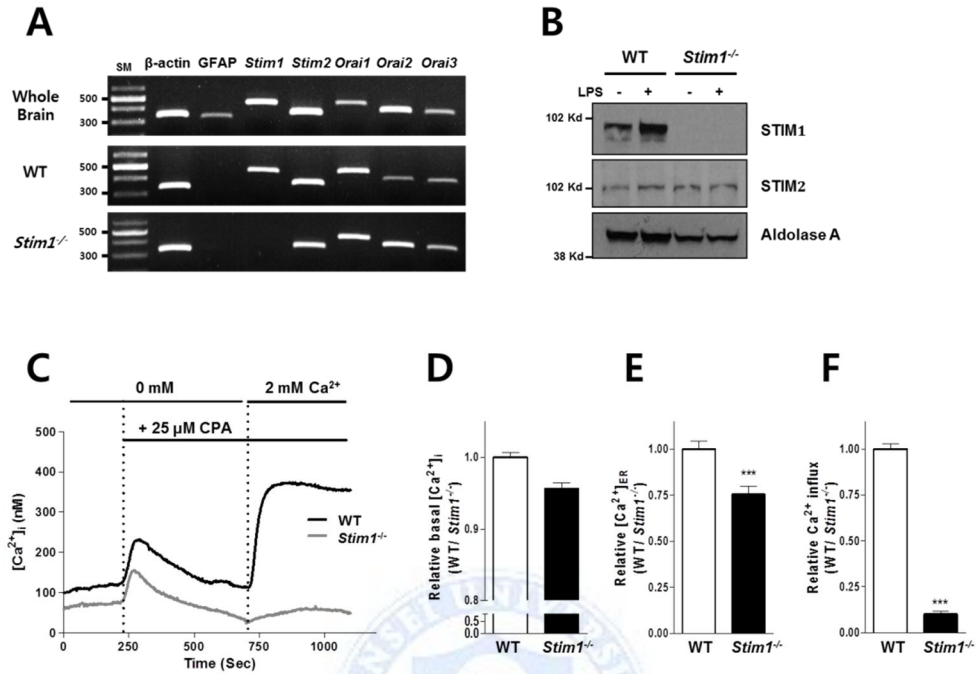
Figure 1. Expression of mRNA and functioning of SOCE elements in primary cultured microglia from WT and *Stim1*^-/- mice. (A) Expression of mRNA transcripts for members of the *Orai*- and *Stim*- families in purified WT and *Stim1*^-/- microglia. Whole mouse brain extract was used as a positive control for RT-PCR; *β*-actin was used as loading control for cDNA. **(B)** STIM1 and STIM2 proteins were identified by immunoblotting in lysates of purified microglia from WT and *Stim1*^-/- mice. Aldolase A was used for loading control. **(C)** Single live cell $[Ca^{2+}]_i$ imaging was monitored as described in the Material and methods section. CPA-induced $[Ca^{2+}]_i$ changes in WT and *Stim1*^-/- microglia are depicted. Representative traces are shown, giving the $[Ca^{2+}]_i$ in each cell measured using Fura-2 AM. Cells were treated with 25 μM CPA to deplete internal Ca^{2+} stores, and then SOCE was monitored in a 2 mM Ca^{2+} perfusion solution. **(D)** Comparisons between WT and *Stim1*^-/- microglia of the basal $[Ca^{2+}]_i$, **(E)** the relative internal Ca^{2+} store amounts calculated by CPA-evoked Ca^{2+} peaks, and **(F)** the CPA-induced SOCE activity as calculated from the slope of Ca^{2+} influx. ***$P \leq 0.0001$ relative to WT values (n>30), and at least three independent experiments were used to calculate the average.

21

2. Comparisons of LPS-stimulated phagocytosis and cytokine secretion between WT and *Stim1⁻ᐟ⁻* microglia

LPS is a potent immune activator of microglia, which binds to TLR4 and activates receptor signaling.[23] The effects of STIM1 on microglial immune function, phagocytic activity, and cytokine secretion was compared between WT and *Stim1⁻ᐟ⁻* microglia.[18] To assess phagocytic activities in WT and *Stim1⁻ᐟ⁻* microglia after differentiation, both resting and LPS-treated (100 ng/ml for 24 hr) cells were compared for their ability to engulf *E.coli* opsonized with FITC-labeled bio-particles. Microglial were treated with bio-particle beads for 2 hr. Then, free beads and attached beads on the cell surface were quenched by trypan blue, and beads inside of cells were visualized using fluorescence microscopy (Fig. 2A, B). In WT cells, LPS treatment for 24 hr increased phagocytic activity approximately 2.5-fold. In contrast, *Stim1⁻ᐟ⁻* microglia only showed small increases in phagocytic activity following LPS treatment. These results clearly demonstrated that the magnitude of phagocytic activity following differentiation by LPS, was decreased in *Stim1⁻ᐟ⁻* microglia.

Next, we compared LPS-induced secretion of the pro-inflammatory cytokines, TNF-α and IL-6 (Fig. 2C, D). The results showed that the amount of these cytokines secreted by *Stim1⁻ᐟ⁻* microglia was less than half the amount secreted by WT microglia. These data indicate that the absence of STIM1 leads to reduced phagocytic activity and cytokine section in microglia differentiated by LPS.
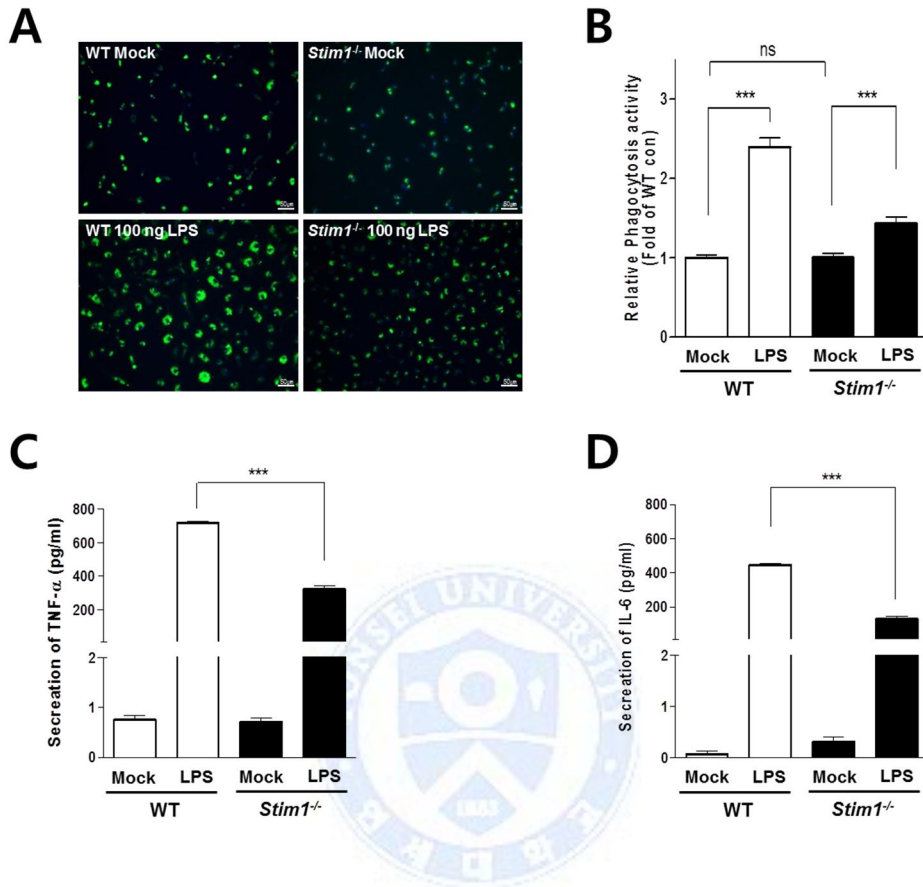
Figure 2. Comparisons of LPS-induced phagocytosis and cytokine secretion between WT and *Stim1⁻ᐟ⁻* microglia. (A) Representative images of the compared phagocytosis measurements. **(B)** Summary of five independent phagocytosis measurements. Seven images were used for phagocytosis measurements and then depicted as a bar graph. ***$P \leq 0.0001$ in LPS-induced fold-induction of WT, n=7. Comparisons of LPS-induced cytokine secretion activity: **(C)** TNF-α secretion and **(D)** IL-6 secretion were compared in WT and *Stim1⁻ᐟ⁻* microglia. ***$P \leq 0.0001$, n=4; (ns, no significant difference from WT mock).

3. Impairment of UDP-induced phagocytosis in *Stim1*^{-/-} microglia

Phagocytosis is activated primarily by the expression of "eat-me" signals on the surface of damaged or dead cells. Injured neurons leak diffusible UDP, which acts as a signal to activate P_2Y_6-dependent phagocytic signaling in microglia[33,54,55]. UDP, which also acts on G_q-coupled P_2Y_6 receptors, induces the expression of chemokines.[56] In contrast to the positive effect of P_2Y_6, stimulation of P_2X_7 or P1 receptors attenuates microglial phagocytosis.[57,58] We first established the mRNA levels of P_2X_4, P_2X_7, P_2Y_6, P_2Y_{12} receptors in primary cultured WT and *Stim1*^{-/-} microglia (Fig. 3A). We measured dose-dependent UDP-induced (at 0.1, 1, 10, 100 μM) $[Ca^{2+}]_i$ increases in WT and *Stim1*^{-/-} microglia (Fig. 3B). In WT microglia, the $[Ca^{2+}]_i$ was increased by UDP in a dose-dependent manner, but *Stim1*^{-/-} microglia did not show any such increase in the $[Ca^{2+}]_i$, due to depletion of the internal Ca^{2+} store. As expected, *Stim1*^{-/-} microglia did not show any sustained Ca^{2+} influx after an initial UDP-induced transient increase in the $[Ca^{2+}]_i$ (Fig. 3C-E). These results confirm that the P_2Y_6-induced Ca^{2+} release from the ER induces the store depletion-mediated Ca^{2+} influx, has been abolished in *Stim1*^{-/-} microglia. Microglia express many of the P2 purinoceptors; P2X receptors, ionotropic receptors, which can be opened mainly by the binding of ATP, and P2Y receptors, metabotropic receptors, which can bind either purines or pyrimidines and activate downstream signaling cascades through G-proteins.[23,59] The P_2X_4, P_2X_7 and P_2Y_{12} of microglia are activated by ATP,[49] and these cells also express the P_2Y_6 receptor which activated by UDP.[33,56]

To examine microglial phagocytosis activity precisely, we used using FACS (Fluorescence-Activated Cell Sorting) to measure the phagocytic engulfment of *E.coli* that had been opsonized with FITC-labeled bio-particles (Fig. 3F, G). After phagocytic beads engulfment for either 20 or 40 min, with or without UDP, microglia were detached by trypsin, and then the fluorescence from beas in each cell was counted by FACS. Fig. 3F shows representative FACS images for WT and *Stim1*^{-/-} microglia. A summary of the phagocytosis of WT and *Stim1*^{-/-} microglia after 20, 40 min of UDP treatment, is presented in Fig. 3G. As can be seen, *Stim1*^{-/-}

microglia had severe defects in UDP-induced phagocytosis. These data establish that STIM1 is a major frontline component of the UDP-induced phagocytosis process *via* its regulation of Ca^{2+} signaling following purinergic receptor activation.
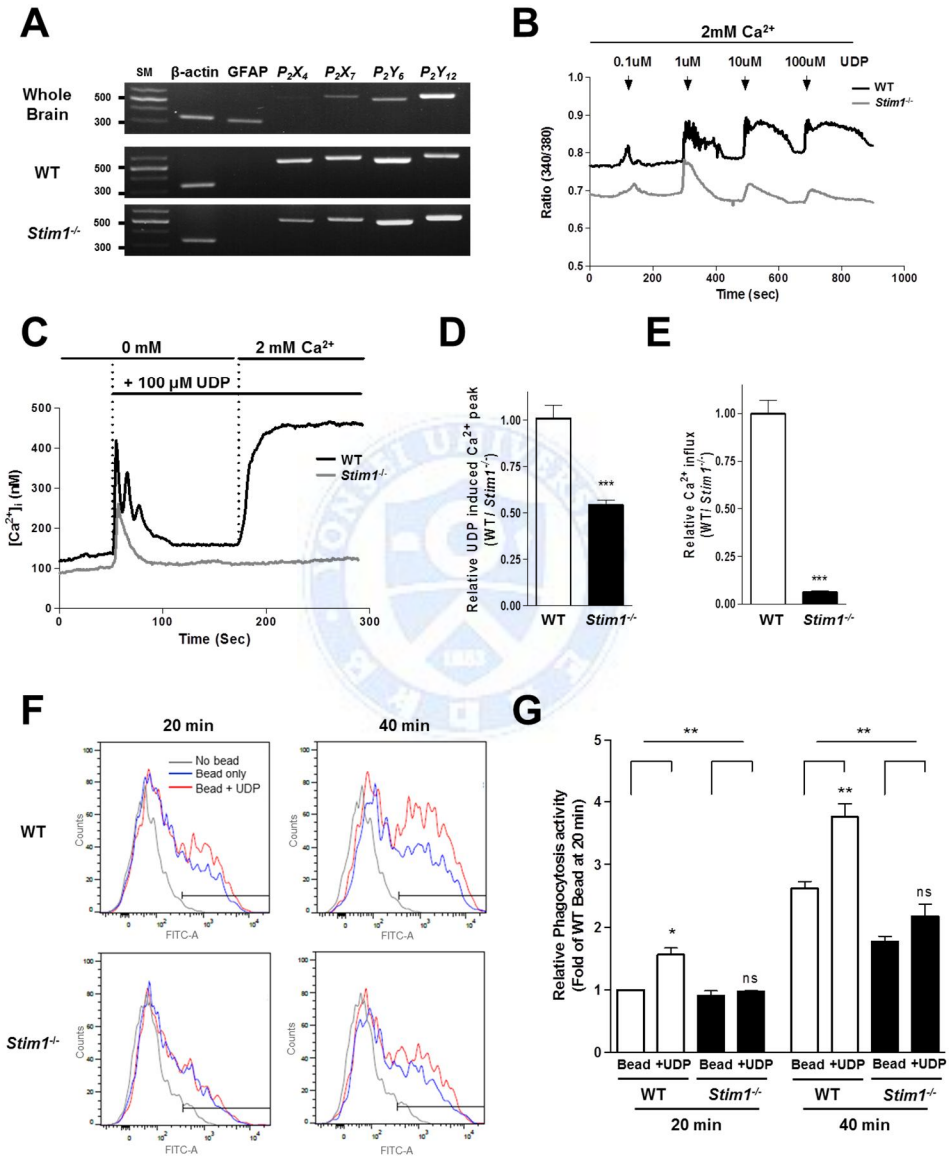

Figure 3. UDP-induced Ca^{2+} signaling and phagocytosis in WT and *Stim1*-/- microglia. (A) The mRNA level of P2 receptors was measured *via* RT-PCR analysis.

(B, C) Single live cell imaging of the $[Ca^{2+}]_i$ was monitored as described in Material and methods section. Each curve represents intracellular Ca^{2+} concentrations ($[Ca^{2+}]_i$) during the experiments. **(B)** Representative trace of dose-dependent UDP-induced transient Ca^{2+} releases from the ER store in WT and *Stim1*$^{-/-}$ microglia. **(C)** Representative curves of 100 μM UDP-induced intracytoplasmic Ca^{2+} mobilization in WT and *Stim1*$^{-/-}$ microglia; 100 μM UDP-induced Ca^{2+} release from the ER, upon store depletion Ca^{2+} influx occurred. **(D)** Quantification of the relative UDP-induced transient Ca^{2+} released from the ER. ***$P \leq 0.0001$, n=15. **(E)** Comparison of UDP-induced SOCE activity calculated from the slope of the Ca^{2+} influx. ***$P \leq 0.0001$, n=15. **(F)** Representative flow cytometry images of the phagocytosis measurements. The intensity of FITC following phagocytic beads engulfment, in the presence of absence 100 μM UDP, was measured at 20 and 40 min. Fluorescence profiles for each group of cells are shown [no beads (black), beads only (blue), and beads + UDP (red)]. High fluorescence populations (gated region) were interpreted as beads engulfing cells. **(G)** Summary of FACS from three independent phagocytosis experiments. The geometric mean in the gated region represents the relative phagocytic activity in each set. **$P \leq 0.001$ in comparison to beads engulfment by WT microglia.

4. Severe defects in the chemotaxis of *Stim1*$^{-/-}$ microglia *in vitro* and *in vivo*

Low ATP concentrations almost universally activate immune cell chemotaxis, in order to attract cells to the site of injury or inflammation.[49] Conversely, when the ATP concentration increases, additional immune effector functions, such as phagocytosis and cytokine secretion, are triggered.[48,49,55,60,61] To compare the ATP-induced Ca^{2+} signaling in WT and *Stim1*$^{-/-}$ microglia, we monitored the $[Ca^{2+}]_i$ by measuring Fura-2 AM fluorescence following the addition of 50 μM ATP (Fig. 4A). Changes in the $[Ca^{2+}]_i$ were calculated by measuring the area under the curve

(AUC), which quantified the magnitude of Ca^{2+} influx upon ATP stimulation. Relative to WT cells, *Stim1*$^{-/-}$ microglia experienced a smaller Ca^{2+} influx (Fig. 4B).

Next, we performed *in vitro* chemotaxis experiments by stimulating with 50 μM ATP (Fig. 4C).[48,49,51,61] The number of cells that had migrated into the ATP chamber, after 15, 30, 60, and 90 min, were subsequently counted by DAPI staining. The extent of WT microglial migration increased in a time-dependent manner. In contrast, *Stim1*$^{-/-}$ microglia did not show a time-dependent increase in migration, and the number of such cells found bottom of chamber was about one-third of the number recorded for the WT cells. These results demonstrate that *Stim1*$^{-/-}$ microglia have severe defects in their chemotatic response to ATP.

To test the *in vivo* behavior of *Stim1*$^{-/-}$ microglia in brains, we injected 30 *nl* of LPS mixed with methylene blue in the 17 day old embryo brains.[53] Methylene blue was used to detect the injection site in brain slices. A full 24 hr after injection, each of embryo brains were harvested and their genotypes were checked. WT and *Stim1*$^{-/-}$ brains were sectioned to 16 μm slices, and those sections marked with methylene blue were selected and stained with Iba-1 to visualize microglia. Fig. 4D shows representative WT and *Stim1*$^{-/-}$ brain slice images under differing levels of magnification.

In the WT brain, Iba-1 positive cells had aggregated around the injected LPS lesion, but the counterpart region of the non-injected hemisphere showed normal ramified microglia. High-magnification images of both sides showed the distinctive morphologies of microglia in the ramified/resting and amoeboid/activated state. In the case of *Stim1*$^{-/-}$ brain tissue, only a few microglia had crowded in the LPS lesions. Although lesion-localized *Stim1*$^{-/-}$ microglia had a similar amoeboid shape as the WT cells, *Stim1*$^{-/-}$ brain slices showed distinctly decreased numbers of microglia aggregated in lesion; suggesting that *Stim1*$^{-/-}$microglia have a defect in migration activity toward injured regions (Fig. 4E).

In the injected legions, the morphology of microglia, which represents the level of differentiation, was almost identical in WT and *Stim1*$^{-/-}$ microglia when their roundness was compared by shape factor (Fig. 4F). We intended to calculate the

extent of phagocytic engulfment of methylene blue particle inside the microglia, but we were unable to measure them because the exposed areas of microglia containing engulfed methylene blue particles were not uniform. These data illustrated that *Stim1*^{-/-} microglia have severe defects in migration, among other immunological activities, and that STIM1 is crucial for microglial chemotaxis *in vitro* and *in vivo*.
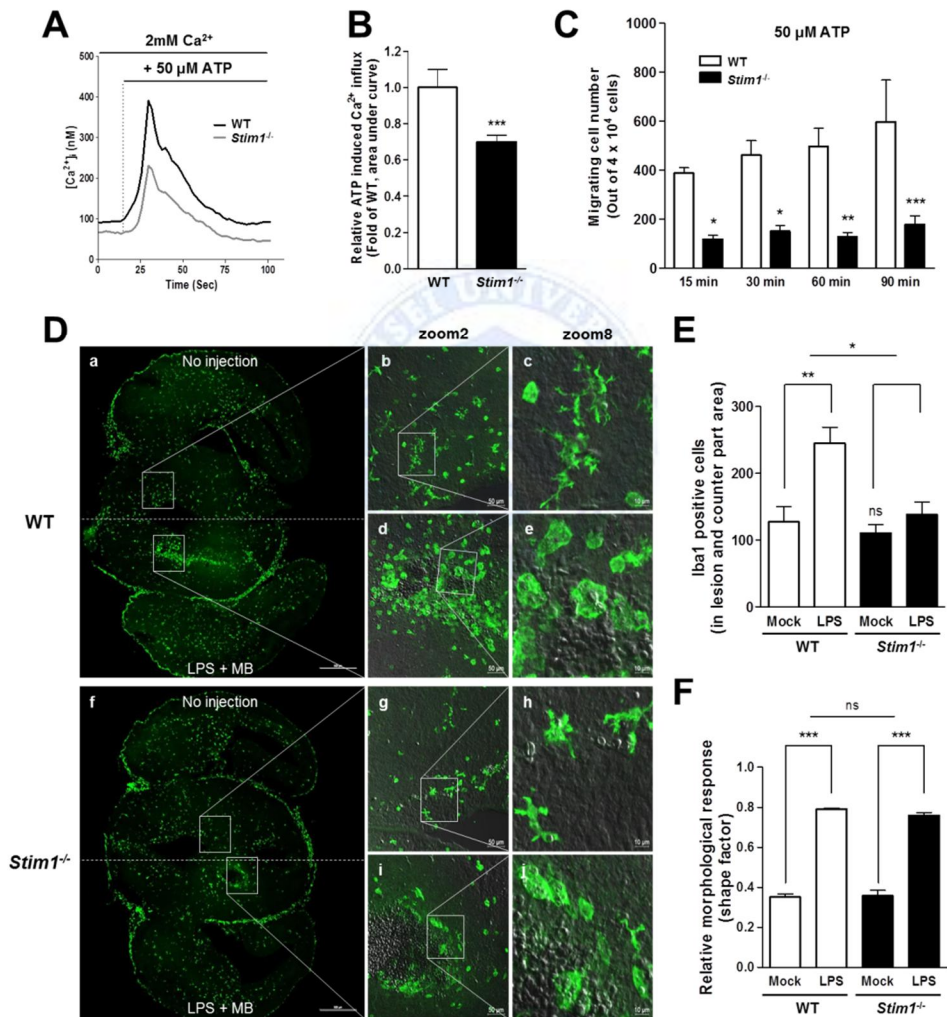

Figure 4. Chemotaxis of WT and *Stim1*^{-/-} microglia *in vitro* and *in vivo*. (A) Single live cell $[Ca^{2+}]_i$ imaging was monitored. Representative curves of 50 μM

ATP-induced mobilization of intracytoplasmic Ca^{2+} in WT and $Stim1^{-/-}$ microglia. $Stim1^{-/-}$ microglia had lower elevations in the $[Ca^{2+}]_i$ than WT cells. **(B)** The relative ATP-induced Ca^{2+} magnitude derived from the area under the curve. ***$P \leq 0.0001$, n>30. **(C)** Time-dependent migration toward 50 μM ATP determined in chemotaxis chambers. Cells that had migrated towards the ATP source were fixed and stained with DAPI and were counted. The number of migrated cells at each time point was determined from six independent experiments and is depicted graphically. *$P \leq 0.005$, **$P \leq 0.001$ and ***$P \leq 0.0001$ *versus* the corresponding control (two-way ANOVA, n=6). **(D)** Microglial aggregation at the site of LPS/methylene blue (MB) injection in embryonic brains of WT and $Stim1^{-/-}$ mice. No LPS injection (upper right hemisphere) and LPS-injected (lower left hemisphere) are indicated in low-magnification images with immunostaining by Iba-1 antibody. Merged images of Iba-1- FITC and gray-DIC are shown in b-e and g-j; microglia are shown in green and methylene blue particles are shown in gray. Resting/ramified microglia (b, c, g, h) were identified in the non-injected hemisphere, and the amoeboid shapes of differentiated microglia engulfing methylene blue particles (d, e, i, j) were identified only in the region injected with LPS + MB. **(E)** The number of Iba-1 positive microglia was counted at the LPS + MB injection site and in the non-injected site. **(F)** Relative morphological changes of WT and $Stim1^{-/-}$ microglia *in vivo*. Shape factors of microglia at the LPS injection site were determined and compared (a circle has a shape factor = 1). *$P \leq 0.05$; (ns, no significant difference from WT mock). Data are representative of three experiments.

5. Formation of ORAI1 surface-clusters is mediated by STIM1 upon internal Ca²⁺ store depletion

To figure out how co-operative between STIM1 and ORAI1 in microglia, we visualized the STIM1 and ORAI1 localization in WT and *Stim1⁻/⁻* microglia under store-depleted (Fig. 5, 6). To detect functional ORAI1 at the cell surface, an antibody recognizing extracellular loop of ORAI1 was used under non-permeabilizing conditions, which did not allow antibody penetration into cells. After ORAI1 labeling with primary and secondary antibodies, cells were permeabilized and STIM1 was labeled.

Resting WT microglia had small clustered STIM1 and ORAI1 structures, only some of them were co-localized at the resting condition. However, the cluster sizes of both proteins increased within 10 min after treatment with 1 μM TG and their co-localization was increased. Most interestingly, in increased cluster size of ORAI1 in response to TG stimulation was dramatically increased in WT microglia (Fig. 5A, D) and the increased ORAI1 clusters were co-localized with the increased STIM1 clusters (Fig. 5C, 6C). Unexpectedly, ORAI1 at the cell surface also increased in *Stim1⁻/⁻* microglia after TG stimulation (Fig. 5B, E). However, the increase cluster size of ORAI1 was not observed. These results offered that the only the clustered ORAI1 co-localized with STIM1 was functional in global $[Ca^{2+}]_i$ increment (Fig. 5D). These results show that STIM1 and ORAI1 work in co-operative upon store depletion conditions. In addition, ORAI1 localization at the cell surface is possible without STIM1, but STIM1 is obviously required for functional ORAI1 increasing global $[Ca^{2+}]_i$.
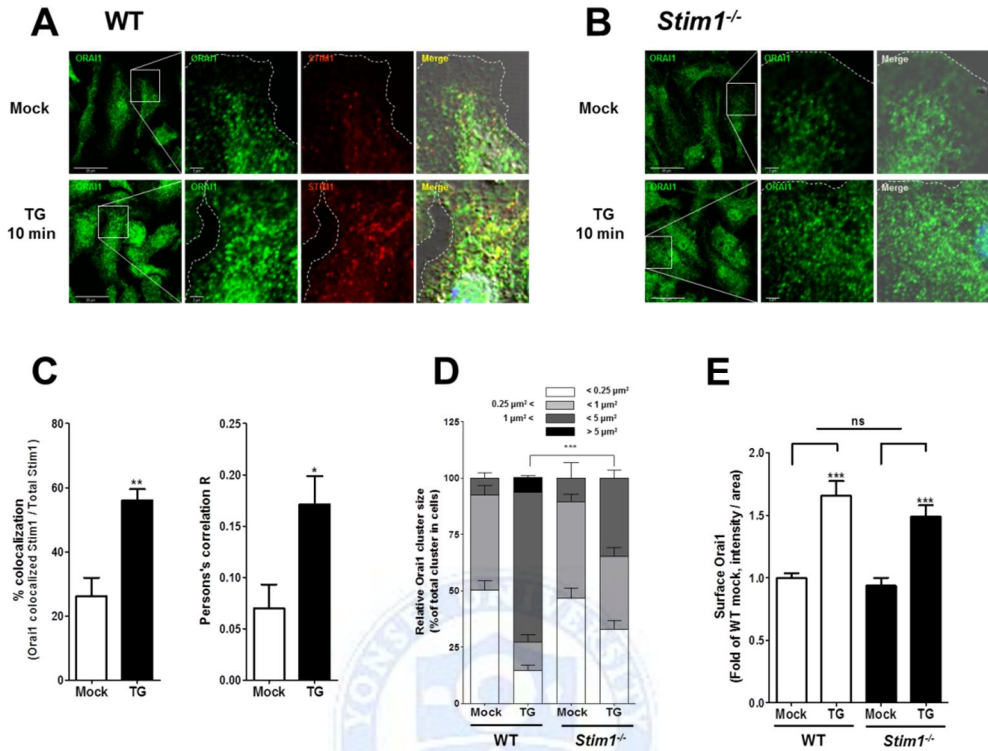
Figure 5. STIM1 is required for the formation of ORAI1 surface-cluster, but not for ORAI1 insertion into the plasma membrane in microglia. (A, B) Surface ORAI1 (green) and STIM1 (red) were immunostained and visualized with confocal microscopy under non-permeabilising immunostaining using an antibody specific for the extracellular loop of ORAI1 (Alomone); STIM1 was subsequently immunolabeled after cell permeabilization in WT microglia and *Stim1*^{-/-} microglia treated with TG (1 μM for 10 min). Insets are high-magnification excerpts from the whole-cell images (Bar=20, 5 μm) to show co-localized clusters (yellow spots; Bar=2, 1 μm). In each panel, the left image shows low-magnification visualization of the gross ORAI1 distribution in cells (Bar=20 μm), and the next three (WT) and two (*Stim1*^{-/-}) high-magnification images show details of cluster size and distribution of each protein; merged images show co-localized protein clusters (yellow spots). Dotted lines indicate the cell border in each image. **(A, C)**

Thapsigargin (TG) induced co-localization of STIM1 and ORAI1 in WT microglia. **(B, E)** Treatment with 1 μM TG for 10 min increased ORAI1 localization at the cell surface throughout the cell border in WT and *Stim1*$^{-/-}$ microglia, **(D)** but ORAI1 clusters co-localized with STIM1 clusters increased in size only in WT microglia

6. Peripheral/central localization of ORAI1 is controlled by STIM1 under UDP/LPS-stimulation

To test whether the central or peripheral localization of ORAI1 was controlled by STIM1, we compared localization of ORAI1 under UDP or LPS treatment which induce acute phagocytic movement and chronic differentiation of microglia through alterations in gene expression, respectively.[62] During the resting state, ORAI1 was only found at the cell periphery. After 40 min UDP treatment, ORAI1 clusters in peripheral region were significantly increased and some of them were co-localized with STIM1 clusters in WT microglia (Fig. 6A). Such clusters of ORAI1 in peripheral regions were not observed in *Stim1*$^{-/-}$ microglia (Fig. 6B).

The opposite phenomenon was observed in LPS-stimulated conditions. LPS treatment for 90 min caused dramatic re-localization of STIM1 and ORAI1 to the cell center near the nucleus, which may cause efficient and marked increase of $[Ca^{2+}]_i$ in WT microglia (Fig. 6D). By contrast, *Stim1*$^{-/-}$ microglia exhibited relatively diffuse ORAI1 localization throughout the cell, and the LPS-induced re-localization of STIM1 and ORAI1 to the cell center was not as profound as that seen in the in WT cells (Fig. 6E). The intensity of surface ORAI1 in the cell periphery was calculated from the intensity of ROIs (0.65 μm away from the edge of cell) using *MetaMorph* software. (Fig. 6C, F). These results suggested that STIM1 is important for ORAI1 localization near the nucleus, which drives a global increase in the $[Ca^{2+}]_i$ in response to LPS stimulation. Moreover, STIM1 is crucial for ORAI1 localization in the cell periphery $[Ca^{2+}]_{micro-domains}$ that controls fast and transient Ca^{2+} signaling required for phagocytic movement.
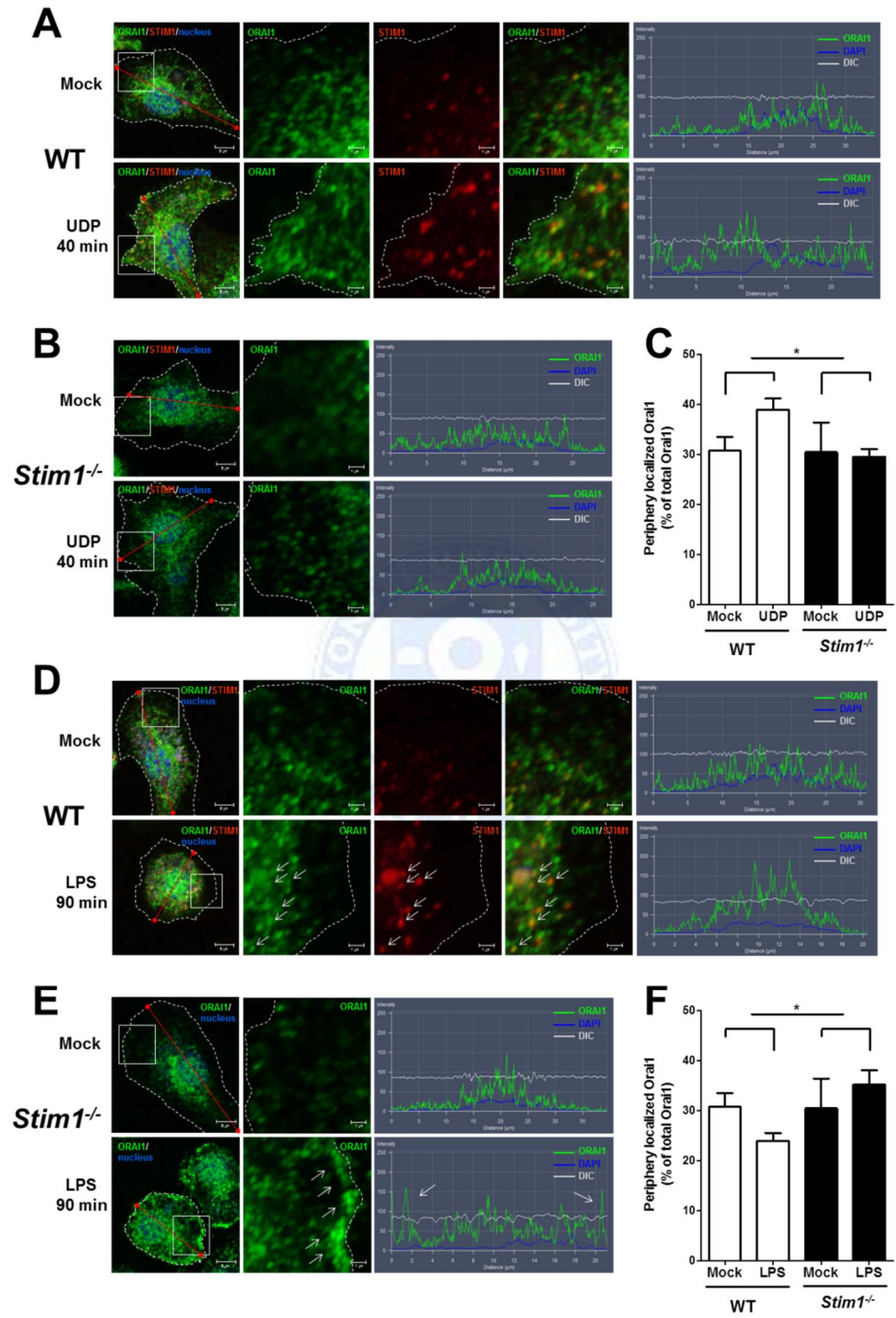
Figure 6. STIM1 controls ORAI1 localization at the cell periphery. (A-C) UDP and **(D-F)** LPS induce co-localization of STIM1 and ORAI1 in WT microglia **(A, D)** and *Stim1$^{-/-}$* microglia **(B, E),** respectively. Treatment with 100 μM UDP for 40 min increased ORAI1 localization at the cell surface throughout the cell border **(A)** in WT and **(B)** *Stim1$^{-/-}$* microglia. Insets were magnified in the remaining images **(A, D)** and **(B, E).** The ORAI1-FITC intensity profile (red lined region) is shown in each of the right-most images. The cell border iss signified by dotted lines and clustered ORAI1 is indicated by arrows. **(C, F)** The intensity of surface ORAI1 in the cell periphery was compared **(C)** in UDP or **(F)** LPS treated cells. The intensity of surface ORAI1 in cell periphery was calculated from the intensity of ROIs, (0.65 μm away from the edge of cell) using *MetaMorph* software.

7. The local [Ca^{2+}]$_{micro-domains}$ fluctuates in *Stim1$^{-/-}$* microglia

Intracellular Ca^{2+} is the principal factor for migration of both immune and cancer cells.[36,63] Local and short-lived micro-domains contain high concentrations of Ca^{2+} cations, sometimes called 'calcium flickers'. The sophisticated spatiotemporal configuration of Ca^{2+} micro-domains can harmonize complicated cellular processes such as cell migration.[36,64,65] In the migrating cell, the Ca^{2+} concentration creates a local Ca^{2+} gradient.[64] Both local and global Ca^{2+} concentrations exert a considerable impact upon cellular functions. We also showed that the migration activity was reduced in *Stim1$^{-/-}$* microglia using a chemotaxis chamber *in vitro* (Fig. 4C) and in *Stim1$^{-/-}$* embryonic brains using microinjection *in vivo* system (Fig. 4D-F). Since the *Stim1$^{-/-}$* microglia abolish acute movements, such as migration and phagocytosis, we routinely observed the changes of [Ca^{2+}]$_i$ after 50 μM ATP (Fig. 7A, B) or 100 μM UDP-stimulations (Fig. 7C, D) using single live cell [Ca^{2+}]$_i$ imaging. After that we visualized the combined images using *MetaMorph* software and found the generation of '*local Ca^{2+} concentration micro-*

domains in the cell periphery' (referred to hereafter as 'local $[Ca^{2+}]_{\text{micro-domains}}$') was noticeably higher in *Stim1$^{-/-}$* microglia than in WT cells (Fig. 7B, D; see the combined images $\sum \Delta F$, right). Then, we measured not only the global change in the $[Ca^{2+}]_i$ (thick black line in trace) in single whole cells (white dotted lines in DIC or ratio images, Fig. 8), but also the local $[Ca^{2+}]_{\text{micro-domains}}$ in both WT (Fig. 8A) and *Stim1$^{-/-}$* microglia (Fig. 8B, 9A). ROIs are colored by ratio, and are depicted alongside the matching color curves to show the changes in peripheral regions. Most strikingly, we noticed a surprising feature in the pattern of Ca^{2+} movements. These showed sporadic and jerky movements in cell periphery of *Stim1$^{-/-}$* microglia.
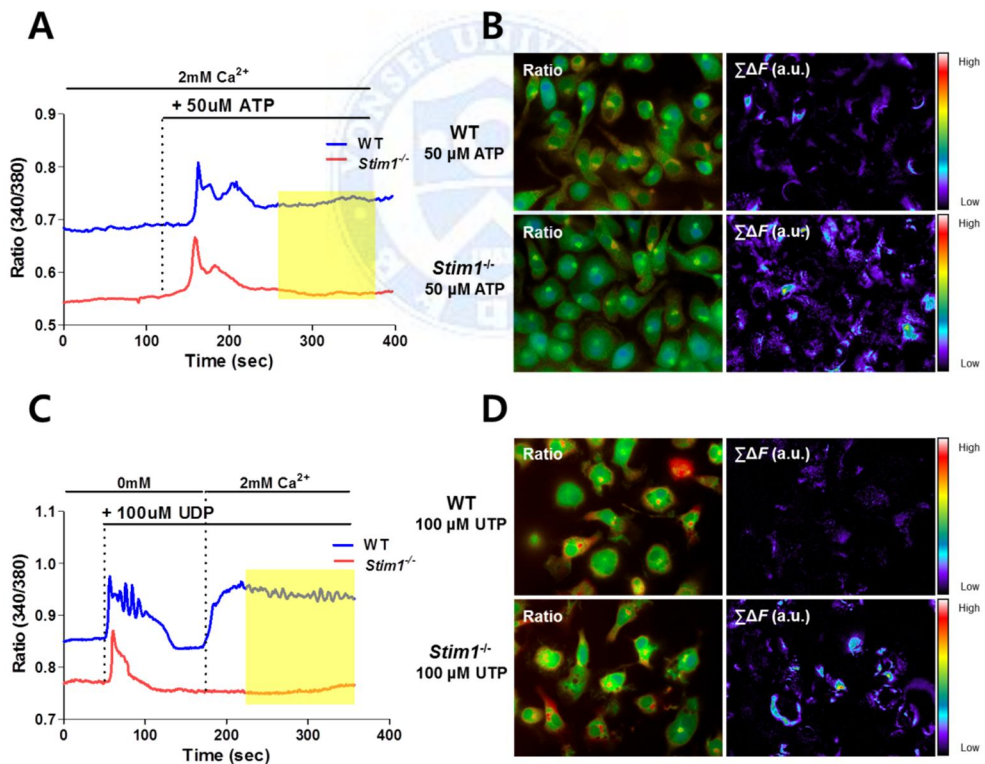

Figure 7. *Stim1$^{-/-}$* microglia showed high $[Ca^{2+}]_{\text{micro-domains}}$ changes in the cell periphery. (A, C) Single live cell $[Ca^{2+}]_i$ imaging was monitored. Representative

curves of **(A)** 50 μM ATP or **(C)** 100 μM UDP-induced $[Ca^{2+}]_i$ mobilization in WT and *Stim1^{-/-}* microglia. The ratio images (340/380 nm, left) and the combined images $\sum\Delta F$ (right) of high-$[Ca^{2+}]_{micro-daomain}$ in cell periphery of WT and *Stim1^{-/-}* microglia after 50 μM ATP **(B)** or 100 μM UDP-stimulation **(D)** were shown; The $\sum\Delta F$ (a.u.) were summed over 27 consecutive images acquired at 8 sec intervals among 108 consecutive images and analyzed by *MetaMorph* software. (a.u.; arbitrary units). The yellow box **(A, C)** indicates the period of $\sum\Delta F$ calculation after 50 μM ATP-stimulation (260–370 sec) and after 100 μM UDP-stimulation (250–360 sec; Fig. 7B, D).
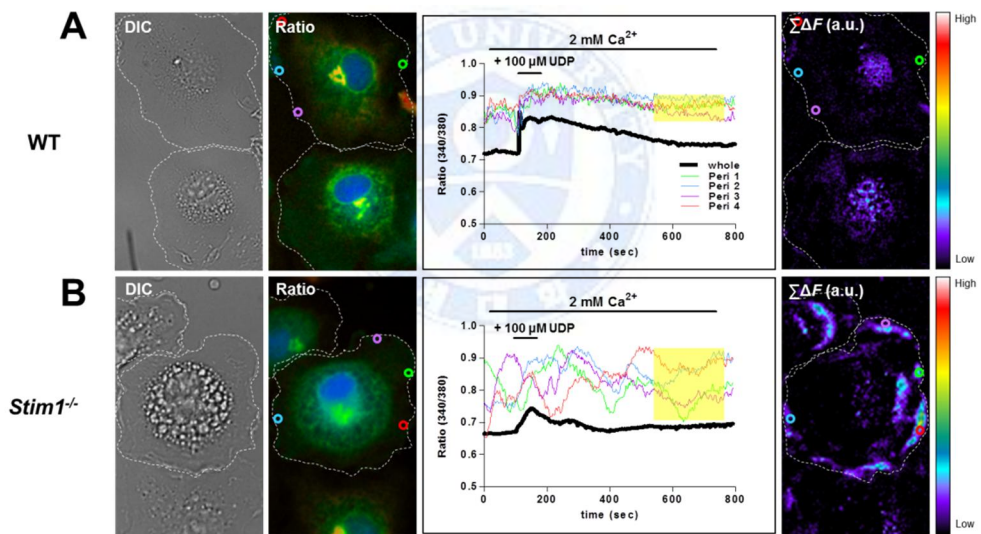
Figure 8. The peripheral region of LPS-stimulated *Stim1^{-/-}* microglial showed a fluctuating local $[Ca^{2+}]_{micro-domains}$. (A, B) Single live cell $[Ca^{2+}]_i$ imaging was monitored. **(A)** WT or **(B)** *Stim1^{-/-}* microglia were initially treated with 100 ng/ml LPS for 90 min, and then stimulated with 100 μM UDP for 1 min in 2 mM Ca^{2+} solution. A single whole cell boundary ROI is shown in white dotted lines on the DIC images. Ratio and $\sum\Delta F$(a.u.) images and representative curves of single whole

cells are shown (thick black line) in ratio images (340/380 nm). Colored ROIs were depicted in cell periphery and matching color-curves show the $[Ca^{2+}]_{micro-domains}$ in corresponding regions. The movements of Ca^{2+} concentration changes ($\sum \Delta F$) were summed over 27 consecutive images acquired at 8 sec intervals among 108 consecutive images during the section of 530–750 (sec) after 100 μM UDP-stimulation for 1 min (Fig. 8, see the ratio of 340/380 nm (left) pattern and combined images ($\sum \Delta F$, right).

8. Fluctuations in the local $[Ca^{2+}]_{micro-domains}$ in $Stim1^{-/-}$ microglia disappear following collapse of the mitochondrial membrane potential

To test the contribution of external Ca^{2+} to the fluctuation of $[Ca^{2+}]_{micro-domains}$ in the peripheral region of $Stim1^{-/-}$ microglia (Fig. 7, 8), we firstly performed that $Stim1^{-/-}$ microglia were firstly treated with 100 ng/ml LPS for 90 min, and stimulated with 100 μM UDP for 1 min in 2 mM Ca^{2+} solution. Then, we changed the bath solution from in 2 mM Ca^{2+} to Ca^{2+}-free with 5 mM EGTA (Fig. 9B). Under the extracellular Ca^{2+}-free conditions, the height of fluctuations in $[Ca^{2+}]_{micro-domains}$ in the cell periphery was slightly reduced, but still clearly showed huge fluctuations of $[Ca^{2+}]_{micro-domains}$ in the cell periphery in $Stim1^{-/-}$ microglia. These data indicate that the main cause of the fluctuating local $[Ca^{2+}]_{micro-domains}$ dose not derive from external Ca^{2+} sources.

The next question we investigated was which intracellular organelles might contribute to this phenomenon. At first, we checked for altered mRNA expression of Ca^{2+} mobilizing proteins in the ER and mitochondria via RT-PCR experiments. Expression of the mRNAs encoding IP_3R-, Ryanodine (Ryr) receptors and $Serca$- in the ER (Fig. 9F, G) and the mRNA expression of the Mcu (mitochondrial Ca^{2+} uniporter), $Ncx1$ (Na^+/Ca^{2+} exchanger), $Letm1$ (Ca^{2+}/H^+ antiporter) and $Vdac$ (voltage-dependent anion channel; one of the component proteins of mitochondrial permeability transition pore [MPTP]) in mitochondria (Fig. 9H) was measured. We

compared these levels and we did not find increases in ER Ca^{2+} mobilizing proteins. However, some of mitochondrial Ca^{2+} mobilizing proteins (MCU, NCX1, Letm1) were notably increased in $Stim1^{-/-}$ microglia. Secondly, we tested the effect on the fluctuating local $[Ca^{2+}]_{micro-domains}$ of inhibiting the IP_3 receptor, which is the main Ca^{2+} mobilizing proteins in the microglial ER; we also tested the effect of two disruptors of the mitochondrial membrane potential. IP_3R inhibition (2-APB; 2-Aminoethyl diphenylborinate, 100 μM) did not have any effect on the fluctuating local $[Ca^{2+}]_{micro-domains}$ in $Stim1^{-/-}$ microglia (Fig. 9C). Surprisingly, however, both carbonyl cyanide 3-chlorophenylhydrazone (CCCP, 0.5 or 1 μM, Fig. 9D) and rotenone (10 μM , Fig. 9E) have a great inhibitory effect on the fluctuating local $[Ca^{2+}]_{micro-domains}$ in $Stim1^{-/-}$ microglia. CCCP is a protonophore which disrupts the mitochondrial membrane potential and rotenone binds to Complex I (NADH dehydrogenase), inhibiting the mitochondrial respiratory chain. These data indicate that the main source of the fluctuating local $[Ca^{2+}]_{micro-domains}$ in microglia derived, not from the ER, but from mitochondria.
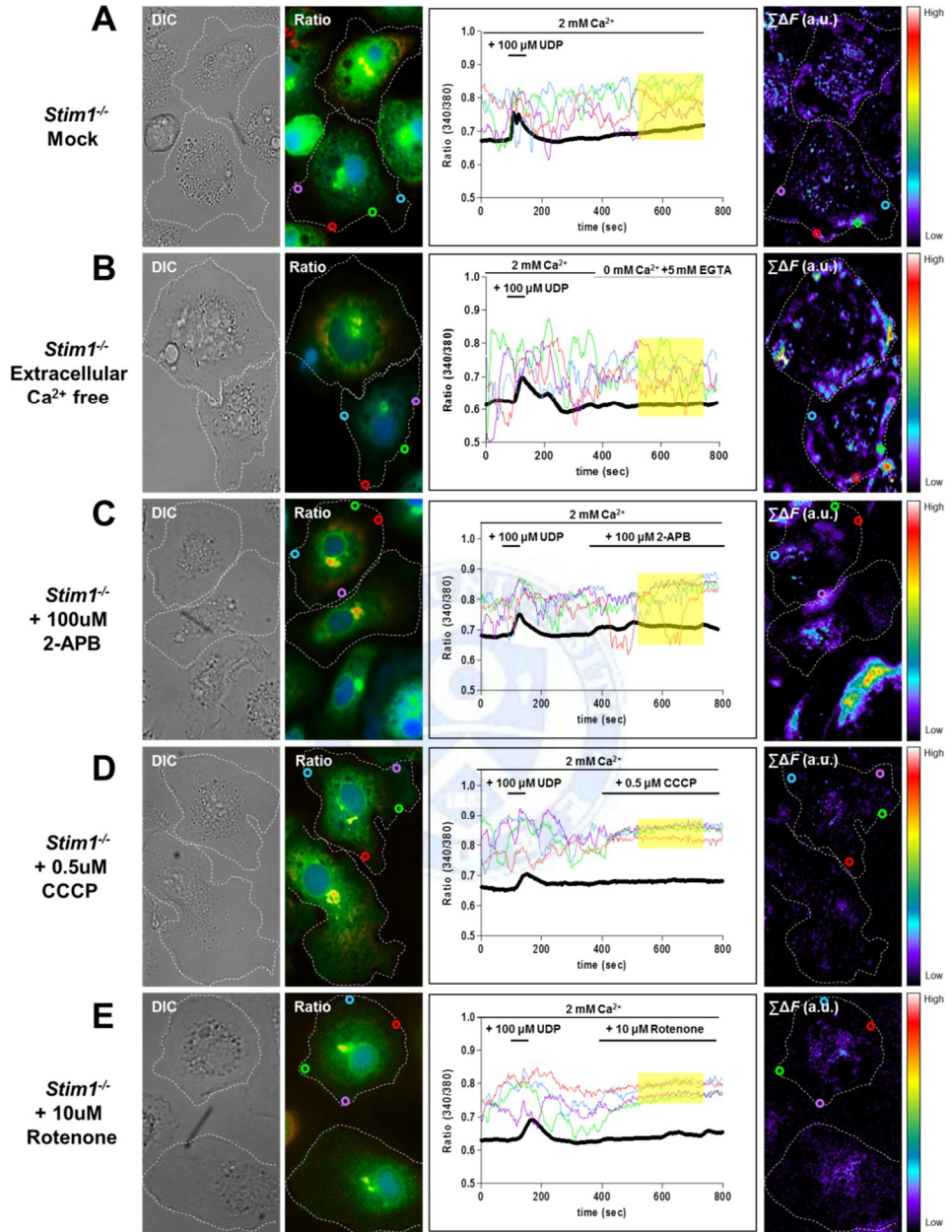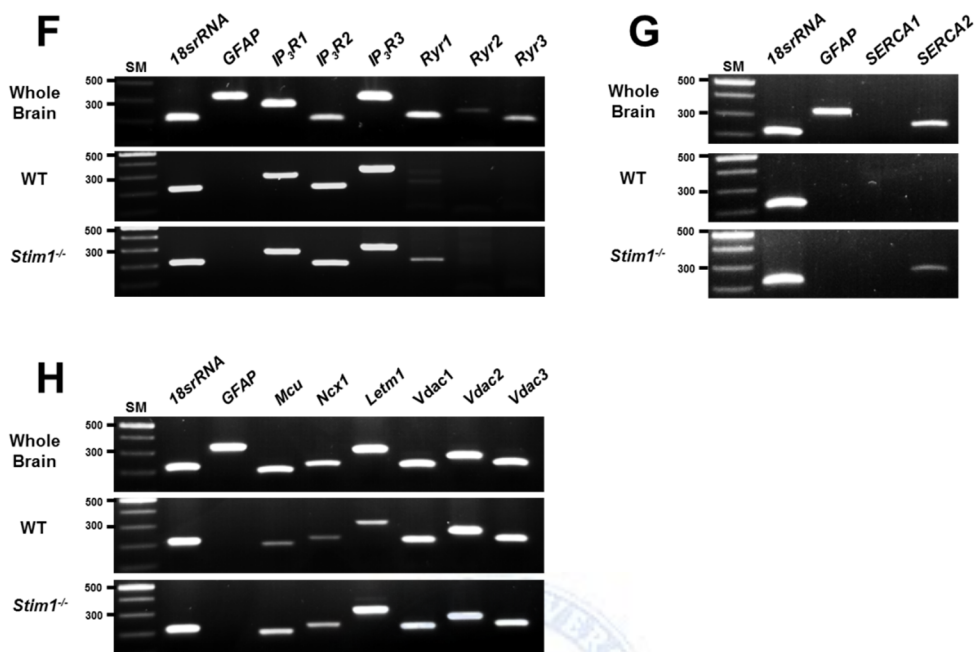
Figure 9. Fluctuations in the local [Ca²⁺]micro-domains in *Stim1⁻ᐟ⁻* microglial disappear following treatment with mitochondrial membrane potential disruptors. (A-E) Single live cell [Ca²⁺]ᵢ imaging was monitored. *Stim1⁻ᐟ⁻* microglia were treated 100 ng/ml LPS for 90 min and then stimulated with 100 μM UDP for 1 min **(A)** in 2 mM Ca²⁺ solution or **(B)** in Ca²⁺-free solution with 5mM EGTA. **(C, D, E)** *Stim1⁻ᐟ⁻* microglia were treated 100 ng/ml LPS for 90 min, and then stimulated with 100 μM UDP for 1 min in 2 mM Ca²⁺ solution. Then inhibitors such as **(C)** 100 μM 2-APB, **(D)** 0.5 μM CCCP and **(E)** 10 μM rotenone were added in 2 mM Ca²⁺ solution, respectively. The combined images (∑ΔF, right) were analyzed during 530-750 (sec). **(F, G)** Expression of mRNA transcripts for members of the *IP₃R-*, *Ryr-* and *Serca-* families in ER, and **(H)** *Mcu*, *Ncx1*, *Letm1*, *Vdac-* in mitochondria in purified WT and *Stim1⁻ᐟ⁻* microglia. Whole mouse brain tissue was used as positive control for RT-PCR; *18srRNA* was used as control for cDNA loading.

40

9. Fluctuations in the local $[Ca^{2+}]_{micro\text{-}domains}$ are influenced by SOCE inhibition

Previously, we showed that ORAI1 localization at the cell surface is increased in *Stim1*^{-/-} microglia (Fig. 5B, E), so we considered what the function of ORAI1 might be when its localization on the cell surface becomes increased, without STIM1. Moreover, Fig. 6E suggested that the LPS treated *Stim1*^{-/-} microglia, large amounts of ORAI1 remained in the peripheral region. These data implied that uncontrolled ORAI1 function may exist in *Stim1*^{-/-} microglia. Furthermore, we previously confirmed that there is a minor reduction in the fluctuations in the local $[Ca^{2+}]_{micro\text{-}domains}$ in *Stim1*^{-/-} microglia when placed in a Ca^{2+}-free solution (Fig. 9B). So, we expected that ORAI1 might have some effect on to the fluctuating local $[Ca^{2+}]_{micro\text{-}domains}$.

To test this hypothesis, we subsequently performed the same experiments, but this time we pre-incubated with Ex-Orai1 antibody or omitted antibody (mock treatment) for 10 min before experiments. The mock set showed a similar pattern to *Stim1*^{-/-} microglia (data not shown), but with the Ex-Orai1 antibody incubation set showed remarkably calm and equable changes in the $[Ca^{2+}]_{micro\text{-}domains}$ in peripheral regions of the cells (Fig. 10B). Additionally, the pharmacological SOC inhibitors, SKF-96365, produced a striking reduction in the fluctuations of the local $[Ca^{2+}]_{micro\text{-}domains}$ (Fig. 10C). However, 200 µM streptomycin (a SACC blocker)[64] did not produced a noticeable change (Fig. 10A), although the mRNA levels of TRPV2, TRPM7, and the SACCs (stretch-activated Ca^{2+} permeant channels of the transient receptor potential superfamily) were clearly detected by RT-PCR (Fig. 10D). These comprehensive results suggest uncontrolled SOCE; and that ORAI1 partially contributes to the fluctuating local $[Ca^{2+}]_{micro\text{-}domains}$ in *Stim1*^{-/-} microglia.
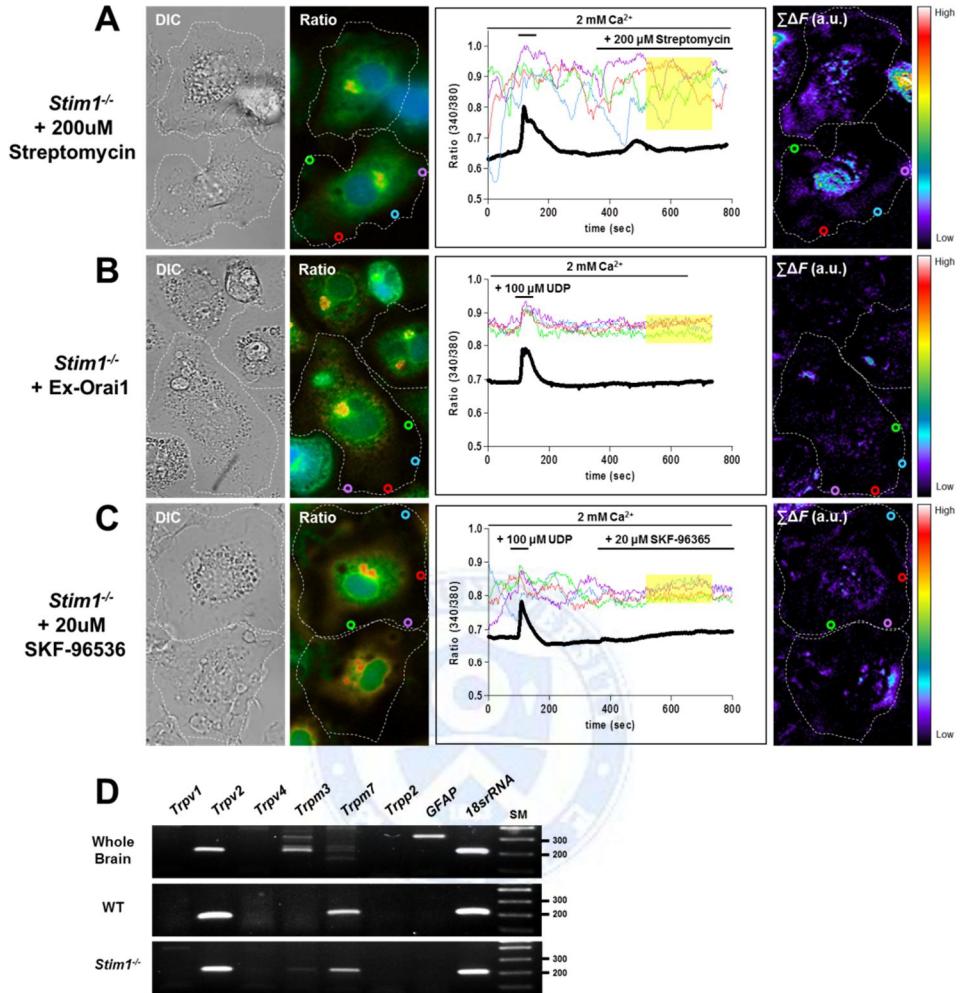
Figure 10. Fluctuations in the local $[Ca^{2+}]_{micro-domains}$ were influenced by SOCE inhibitors. (A-C) Single live cell $[Ca^{2+}]_i$ imaging was monitored. *Stim1^-/-* microglia were pre-treated with 100 ng/ml LPS for 90 min, and then stimulated with 100 μM UDP for 1 min in a 2 mM Ca^{2+} solution. The combined images (∑ΔF, right) were analyzed during 530–750 sec. *Stim1^-/-* microglia were pre-treated 100 ng/ml LPS for 90 min, and stimulated with 100 μM UDP for 1 min in a 2 mM Ca^{2+} solution. Then the cells were placed in a 2 mM Ca^{2+} solution and treated with either **(A)** 200 μM streptomycin, or with **(C)** 20 μM SKF-96365. **(B)** After pre-treatment of LPS, cells were pre-incubated with the extracellular ORAI1 antibody (Ex-Orai1) for 10 min at 37 °C with 5% CO_2 in an incubator, before being stimulated with 100 μM UDP. **(D)**

Expression of mRNA transcripts for members of the SACC families in purified WT and *Stim1$^{-/-}$* microglia. Whole mouse brain extract was used as positive control for RT-PCR; 18srRNA was used as control for cDNA loading.

10. Comparisons of mitochondrial characteristics between WT and *Stim1$^{-/-}$* microglia

Having observed the complete blockage of fluctuations in the local $[Ca^{2+}]_{micro-domains}$ in *Stim1$^{-/-}$* microglia following treatment with either CCCP or rotenone, we set out to phenotypically characterize the mitochondria in both WT and *Stim1$^{-/-}$* microglia using transmission electron microscopy (TEM). To assess the changes in the structural features of mitochondria from WT and *Stim1$^{-/-}$* microglia, including the double layer membrane and cristae, had no discernible differences (Fig. 11A), and total numbers of mitochondria were similar in each cell (Fig. 11B).

However, we tested the mRNA expression of each isoform of the tether proteins; (Mitofusin- and Miro-) using RT-PCR analysis, the levels of *Mitofusin-1*, *Mitofusin-2*, *Miro-1* and *Miro-2* genes are more increased in *Stim1$^{-/-}$* microglia than WT cells (Fig. 11C). These data suggested that STIM1 may participate in the allocation of mitochondria.
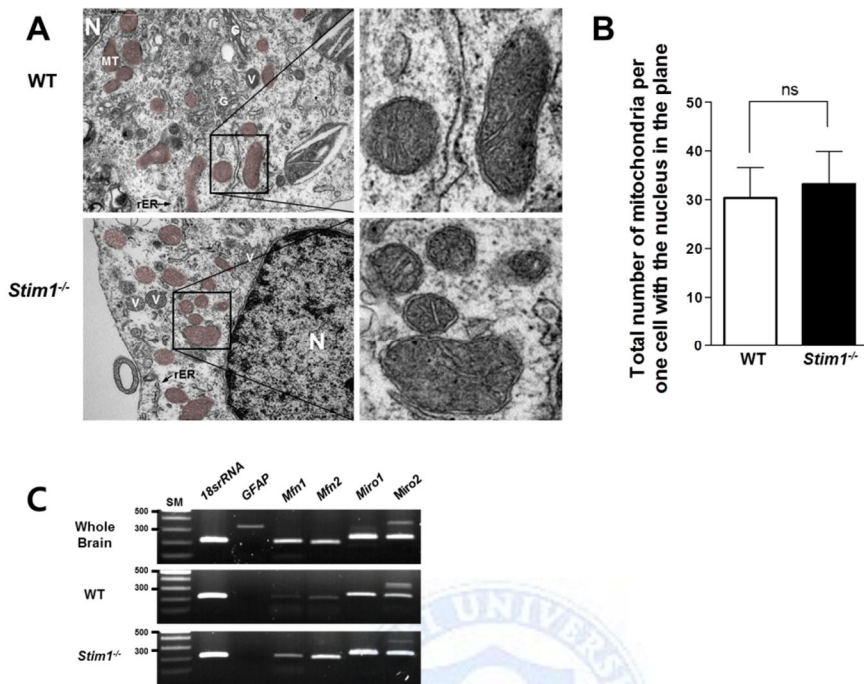
Figure 11. Comparisons of the structure and the total numbers of mitochondria of WT and *Stim1*^{-/-} microglia using TEM. (A) TEM images of WT and *Stim1*^{-/-} microglia. The mitochondria are indicated in pale pink. N = nucleus; MT = mitochondria; G = Golgi apparatus; rER = rough endoplasmic reticulum; V = vacuole. Scale bars; 1000 nm **(B)** The total numbers of mitochondria per cell were counted in the plane of section containing the nucleus. **(C)** Expression of mRNA transcripts for members of the *Mitofusin-* and *Miro-* families in purified WT and *Stim1*^{-/-} microglia. Whole mouse brain extract was used as a positive control for RT-PCR; *18srRNA* was used as loading control for cDNA.

IV. DISCUSSION

Our key findings suggest that, while STIM1-mediated SOCE is certainly important in the regulation of global $[Ca^{2+}]_i$ changes, STIM1 is also the foremost regulator of the local $[Ca^{2+}]_{micro-domains}$ in murine microglia. So, we claim that STIM1 orchestrates the Ca^{2+} signaling that modulates the immune function of murine microglia.

Our current study is largely divided into two parts. In the first part, we studied the global $[Ca^{2+}]_i$ changes influenced by the immunological functions of microglia; such as phagocytosis, cytokine secretion, chemotaxis (both *in vitro* and *in vivo*) following LPS, UDP or ATP-stimulation using primary cultured WT and *Stim1*^{-/-} microglia from C57BL/6 strain mice and the brains of embryonic *Stim1*^{-/-} mice.[6] In the second part, we paid careful attention to the local Ca^{2+} movements in the cell periphery of microglia, since we had established that there were severe defects in their chemotactic activities *in vitro* and *in vivo*.

Initially, we evaluated the role of STIM1-mediated SOCE activation and Ca^{2+} release activated channel (CRAC) activation. STIM2 has less of an effect than STIM1 in T-cells.[5,22] Michaelis *et al*. recently reported that *Stim2*^{-/-} microglia displayed SOCE activation upon store depletion and nucleotide stimulation, in contrast to the complete absence of SOCE in *Stim1*^{-/-} microglia.[20] In spite of the presence of STIM2 (Fig. 1A, B), the western blot analyses and $[Ca^{2+}]_i$ measurements demonstrated that STIM1 is the primary regulator of SOCE in microglia. STIM2 is a feedback regulator that stabilizes the $[Ca^{2+}]_i$ *via* reduction of ER $[Ca^{2+}]$-sensitive translocation to the plasma membrane.[15] We did not detect significant changes in *Stim2* mRNA (Fig. 1A) or STIM2 protein (Fig. 1B) in *Stim1*^{-/-} microglia, and the basal $[Ca^{2+}]_i$ was lower in *Stim1*^{-/-} microglia than in WT (Fig. 1C, D). These result suggest that an increased interaction of STIM2 with Orai isotypes does not induce basal $[Ca^{2+}]_i$ elevation. The current study suggests that STIM1 is the major regulator of SOCE-mediated Ca^{2+} influx and is the critical

determinant of the basal $[Ca^{2+}]_i$ levels in microglia. A principal role for STIM1 in global $[Ca^{2+}]_i$ changes was demonstrated in cells treated with LPS, which activates innate immune functions in microglia. Both basal phagocytosis (Fig. 2A, B) and secretion of the cytokines TNF-α and IL-6 (Fig. 2C, D) following LPS treatment, were reduced significantly in *Stim1*^{-/-} microglia. These data are consistent with the established role of SOCE-mediated global $[Ca^{2+}]_i$, which changes during pro-inflammatory activation of microglia.

Cell migration is coordinated by Ca^{2+} signaling, in part through local Ca^{2+} signaling in the leading cell edge.[36] Previous reports have shown that STIM1 localize to podosomes,[66] phagosomes,[34] and cell-matrix adhesions at the front of migrating cells.[36] Recent work have shown that receptor tyrosine kinase signaling and phospholipase-C signaling are restricted to the front of migrating endothelial leader cells, which triggers local STIM1 activation, local Ca^{2+} pulses and local depletion of ER-Ca^{2+}. These cascades orchestrate pulsatile retraction and adhesion of the leading cell front.[36] Another study reported that STIM1 localization is juxtaposed to the ER and to phagosomes, which generate Ca^{2+} hotspots that boost phagocytosis.[34]

Our results are in agreement with the findings of these previous studies; namely, that STIM1-regulated local Ca^{2+} influx to the leading focal adhesion micro-domains influences for the functions mediated by local cytoskeletal rearrangement. These include a reduction in UDP-induced rapid phagocytosis (Fig. 3F, G) and ATP-induced chemotaxis (Fig. 4C) in *Stim1*^{-/-} microglia. UDP-induced phagocytosis is relatively fast, yet its capacity is comparably smaller, compared to basal phagocytosis of opsonized beads. We demonstrated that phagocytosis is highly dependent on STIM1-mediated Ca^{2+} influx to local micro-domains after P_2Y_6 stimulation because UDP-induced phagocytosis became markedly impaired in *Stim1*^{-/-} microglia. Similarly, time-dependent ATP-stimulated cell migration was essentially abolished in *Stim1*^{-/-} microglia. This *in vitro* result was confirmed in the *in vivo* studies,[53] which showed that cell migration to the injured site was severely impaired in *Stim1*^{-/-} mice (Fig. 4D-F). Injured cells release nucleotides such as ATP,

which is a known chemotactic attractant and an activator of purinergic receptors such as P_2X_4 and P_2Y_{12}, involved in the rapid cell migration fundamental for microglial recruitment to the site of brain lesions.[49,60] The defective chemotaxis of $Stim1^{-/-}$ microglia demonstrated clearly that STIM1 is an essential regulator of chemotaxis governed by local Ca^{2+} micro-domains. These data suggest that the contribution of STIM1 to local Ca^{2+} micro-domains is not negligible in comparison with the global $[Ca^{2+}]_i$ changes. The immunocytochemistry of STIM1 and ORAI1 was compared between WT and $Stim1^{-/-}$ microglia, showing that the efficient and appropriate localization of ORAI1 following stimulation with either LPS or UDP requires STIM1 (Fig. 6). We surmise from our data that STIM1 produces in global $[Ca^{2+}]_i$ changes and it also has a role in regulating local Ca^{2+} micro-domains which are principally responsible for phagocytosis and cytoskeletal rearrangement during stimulus-induced cell movement.

In the migrating cell, a Ca^{2+} concentration gradient forms locally at certain regions of the cell.[64] The research spotlight is now on the notion that 'local Ca^{2+} signals', 'Ca^{2+} micro-domains', or 'local hot spots' of high Ca^{2+} generated by the opening of Ca^{2+} channels in the cell periphery.[37-39,67,68] A role for STIM1 in the migration of various cells is being increasingly reported. Human STIM1 is locally activated in the migrating front HUVEC cells.[36] Another study reported that Ca^{2+} influx mediated by ORAI1 and STIM1 may promote tumor metastasis, migration and invasion. This study also highlighted the interplay between STIM1 and turnover of focal adhesions, which is needed for migration.[63] However, none of these reports suggested the direct requirement of STIM1 in migration, nor did they elucidate the detailed mechanism, nor did they focus on the coordination of Ca^{2+} signaling through controlling $[Ca^{2+}]_{micro-domains}$.

Initially, we found the changes in the local $[Ca^{2+}]_{micro-domains}$ in the cell periphery of $Stim1^{-/-}$ microglia stimulated with 50 μM ATP (Fig. 7A, B) or 100 μM UDP, were noticeably higher than WT (Fig. 7B, D) in combined images($\sum\Delta F$) analyzed by *MetaMorph* software. We measured not only the global change of $[Ca^{2+}]_i$ in the single whole cell, but also the local $[Ca^{2+}]_{micro-domains}$ of WT (Fig. 8A) and $Stim1^{-/-}$

microglia (Fig. 8B, 9A). When we tested the impact of an extracellular Ca^{2+}-free environment on $Stim1^{-/-}$ microglia (Fig. 9B), the local $[Ca^{2+}]_{micro\text{-}domains}$ appeared slightly reduced, yet huge changes of in the local $[Ca^{2+}]_{micro\text{-}domains}$ still occurred. These data hinted that the primary source of the fluctuating local $[Ca^{2+}]_{micro\text{-}domains}$ derives from Ca^{2+} released by intracellular organelles. We confirmed this, since both CCCP (Fig. 9D) and rotenone (Fig. 9E) greatly disturbed the fluctuations in the local $[Ca^{2+}]_{micro\text{-}domains}$ of $Stim1^{-/-}$ microglia. In contrast, the IP_3R inhibitor, 2-APB, had no such effect (Fig. 9C). These data implied that the fluctuating local $[Ca^{2+}]_{micro\text{-}domains}$ in $Stim1^{-/-}$ microglia is generated by mitochondria but not the ER. Interestingly, the transcript levels of *Mcu* (mitochondrial Ca^{2+} uniporter), *Ncx1* (Na^+/Ca^{2+} exchanger) and *Letm1* (Ca^{2+}/H^+ antiporter) are up-regulated in $Stim1^{-/-}$ microglia, but *Vdac-* (voltage-dependent anion channel) is not (Fig. 9H). At present, we cannot conclude that the increased expression of two mitochondrial Ca^{2+} influx proteins is responsible for the fluctuating $[Ca^{2+}]_{micro\text{-}domains}$, so the testing of specific inhibitors against both proteins is warranted in future experiments. In addition, we cannot conclude that their altered expression is caused by the absence of STIM1, including *Mitofusin-* and *Miro-* families, the tether genes (Fig. 11C). Mitofusin-2, the protein which tethers mitochondria to the ER-membrane, is known to be a necessary factor for STIM1 translocation into junction between the ER and the plasma membrane in MEK cells,[44] In spite of this, the molecular mechanism/physical detail of this interaction has not been revealed. Our finding that the allocation of mitochondrial tether genes is affected by STIM1, provides further evidence for the interaction between STIM1 and mitochondria. Moreover, although the detailed mechanism remains vague, inhibition of ORAI1 also reduced the fluctuations in the $[Ca^{2+}]_{micro\text{-}domains}$, which strongly supports the previous reports that mitochondrial Ca^{2+} buffering capacity is influenced by SOCE-mediated Ca^{2+} influx. On the other hand, TEM results showed that the structure of mitochondria is indistinguishable between WT and $Stim1^{-/-}$ microglia (Fig. 11A), and that total numbers of mitochondria were same in both groups (Fig. 11B). The exact cause of the functioning of mitochondria in $Stim1^{-/-}$ microglia will need to be investigated by

further experiments.

These results comprehensively demonstrate that STIM1 is a critical controller of the local $[Ca^{2+}]_{micro-domains}$, not only through regulating local SOCE pores, but also through coordinating the mitochondrial Ca^{2+} buffering capacity in the micro-domains of the cell periphery

The phenomenon of fluctuating $[Ca^{2+}]_{micro-domains}$ in *Stim1*$^{-/-}$ microglia seems to have been veiled so far, due to the general $[Ca^{2+}]_i$ monitoring methods in use, which only monitor the $[Ca^{2+}]$ change throughout the whole cell. Notably, we could capture this local fluctuation in the $[Ca^{2+}]_{micro-domains}$ in *Stim1*$^{-/-}$ microglia using two reliable methods; the measurement of the $[Ca^{2+}]$ through drawing small ROIs only in local regions of cells, and the summation of these $[Ca^{2+}]$ changes during a period of stable $[Ca^{2+}]_i$ in *Stim1*$^{-/-}$ microglia. Of course, although the extremely thin layer of the peripheral region in microglia seems to provide the ideal vantage point to monitor the $[Ca^{2+}]_{micro-domains}$, we have reasons nonetheless to expect that this fluctuating $[Ca^{2+}]_{micro-domains}$ caused by depletion of STIM1 will be seen in many other cell types.

Besides the confirmation that STIM1-mediated SOCE is centrally important in the regulation of global $[Ca^{2+}]_i$ changes in microglia, the distinctiveness of our study lies the novel finding of hitherto unnoticed roles of STIM1 in the regulation of local Ca^{2+} micro-domains in physiological situations. The fluctuating local $[Ca^{2+}]_{micro-domains}$ and severe migration defects in *Stim1*$^{-/-}$ microglia might have a causal relationship, which would suggest that STIM1 is required to stabilize and control the Ca^{2+} signal at the $[Ca^{2+}]_{micro-domains}$ in the cell periphery, allowing coordinated movements in murine microglia. Although we did not elucidate the exact molecular defects in the mitochondrial Ca^{2+} buffering capacity in cells lacking STIM1, our data clearly shed new light on the regulatory function of STIM1 in the local Ca^{2+} signal produced at micro-domains. STIM1 orchestrates this signal, not only *via* local SOCE channels, but also by coordinating the Ca^{2+} buffering capacity of mitochondria near to SOCE pores.

V. CONCLUSION

In the present study, we have focused on the changes in both global $[Ca^{2+}]_i$ by SOCE, and local $[Ca^{2+}]_{micro-domains}$, which are related to chronic and acute movements, respectively, using primary cultured WT and *Stim1$^{-/-}$* microglia. Our current study examined the *in vitro* and *in vivo* effects of STIM1-modulated SOCE in pathogen- or purinergic-mediated immunological functions using microglia from *Stim1$^{-/-}$* mice. STIM1 is the primary determinant of SOCE-mediated Ca^{2+} influx and the main regulator of basal $[Ca^{2+}]_i$ levels in murine microglia. STIM1 is also important for innate immune function such as phagocytosis and cytokine release in LPS-stimulated microglia. We found a reduction of chemotaxis *in vitro* and *in vivo*, which prompted us to visualize the changes in the local $[Ca^{2+}]_{micro-domains}$ in the cell periphery following UDP-stimulation in LPS-activated *Stim1$^{-/-}$* microglia.

Most unexpectedly, *Stim1$^{-/-}$* microglia showed massive changes in the local $[Ca^{2+}]_{micro-domains}$ compared to WT; so we established that the sources of the fluctuating local $[Ca^{2+}]_{micro-domains}$ derive from both inside and outside the cell. Application of the Ex-Orai1 antibody and SKF-96536 (a SOC inhibitor), we concluded that the fluctuating local $[Ca^{2+}]_{micro-domains}$ in *Stim1$^{-/-}$* microglia are partially caused by surface ORAI1. Above all, we confirmed that the main cause of the fluctuation in the local $[Ca^{2+}]_{micro-domains}$ is mediated by mitochondria. That is, STIM1 inhibits the fluctuating Ca^{2+} flickers occurred *via* mitochondria which are capably manage the stability of local Ca^{2+} signals to react immediately upon acute movements in murine microglia.

Taken together, these *in vitro* and *in vivo* results demonstrate that STIM1-mediated SOCE is the decisive factor in the regulation of global $[Ca^{2+}]_i$ changes, and is crucial for the regulation of local $[Ca^{2+}]_{micro-domains}$ in murine microglia. We conclude that STIM1 orchestrates the physiological Ca^{2+} signaling that modulates the immune function of murine microglia.

REFERENCES

1.   Berridge MJ, Bootman MD, Lipp P. Calcium--a life and death signal. Nature 1998;395:645-8.

2.   Parekh AB. Store-operated CRAC channels: function in health and disease. Nat Rev Drug Discov 2010;9:399-410.

3.   Parekh AB, Putney JW, Jr. Store-operated calcium channels. Physiol Rev 2005;85:757-810.

4.   Moller T. Calcium signaling in microglial cells. Glia 2002;40:184-94.

5.   Oh-Hora M, Yamashita M, Hogan PG, Sharma S, Lamperti E, Chung W, et al. Dual functions for the endoplasmic reticulum calcium sensors STIM1 and STIM2 in T cell activation and tolerance. Nat Immunol 2008;9:432-43.

6.   Baba Y, Nishida K, Fujii Y, Hirano T, Hikida M, Kurosaki T. Essential function for the calcium sensor STIM1 in mast cell activation and anaphylactic responses. Nat Immunol 2008;9:81-8.

7.   Putney JW, Jr. Capacitative calcium entry revisited. Cell Calcium 1990;11:611-24.

8.   Vig M, Kinet JP. Calcium signaling in immune cells. Nat Immunol 2009;10:21-7.

9.   Parekh AB, Fleig A, Penner R. The store-operated calcium current I(CRAC): nonlinear activation by InsP3 and dissociation from calcium release. Cell 1997;89:973-80.

10.   Liou J, Kim ML, Heo WD, Jones JT, Myers JW, Ferrell JE, Jr., et al. STIM is a Ca2+ sensor essential for Ca2+-store-depletion-triggered Ca2+ influx. Curr Biol 2005;15:1235-41.

11.   Huang GN, Zeng W, Kim JY, Yuan JP, Han L, Muallem S, et al. STIM1 carboxyl-terminus activates native SOC, I(crac) and TRPC1 channels. Nat Cell Biol 2006;8:1003-10.

12.   Worley PF, Zeng W, Huang GN, Yuan JP, Kim JY, Lee MG, et al. TRPC channels as STIM1-regulated store-operated channels. Cell Calcium 2007;42:205-11.

13. Yuan JP, Zeng W, Dorwart MR, Choi YJ, Worley PF, Muallem S. SOAR and the polybasic STIM1 domains gate and regulate Orai channels. Nat Cell Biol 2009;11:337-43.

14. Soboloff J, Rothberg BS, Madesh M, Gill DL. STIM proteins: dynamic calcium signal transducers. Nat Rev Mol Cell Biol 2012;13:549-65.

15. Brandman O, Liou J, Park WS, Meyer T. STIM2 is a feedback regulator that stabilizes basal cytosolic and endoplasmic reticulum Ca2+ levels. Cell 2007;131:1327-39.

16. Zhang H, Clemens RA, Liu F, Hu Y, Baba Y, Theodore P, et al. STIM1 calcium sensor is required for activation of the phagocyte oxidase during inflammation and host defense. Blood 2014;123:2238-49.

17. Varga-Szabo D, Braun A, Kleinschnitz C, Bender M, Pleines I, Pham M, et al. The calcium sensor STIM1 is an essential mediator of arterial thrombosis and ischemic brain infarction. J Exp Med 2008;205:1583-91.

18. Heo DK, Lim HM, Nam JH, Lee MG, Kim JY. Regulation of phagocytosis and cytokine secretion by store-operated calcium entry in primary isolated murine microglia. Cell Signal 2015;27:177-86.

19. Braun A, Gessner JE, Varga-Szabo D, Syed SN, Konrad S, Stegner D, et al. STIM1 is essential for Fcgamma receptor activation and autoimmune inflammation. Blood 2009;113:1097-104.

20. Michaelis M, Nieswandt B, Stegner D, Eilers J, Kraft R. STIM1, STIM2, and Orai1 regulate store-operated calcium entry and purinergic activation of microglia. Glia 2015;63:652-63.

21. Vaeth M, Zee I, Concepcion AR, Maus M, Shaw P, Portal-Celhay C, et al. Ca2+ Signaling but Not Store-Operated Ca2+ Entry Is Required for the Function of Macrophages and Dendritic Cells. J Immunol 2015;195:1202-17.

22. Oh-hora M, Rao A. Calcium signaling in lymphocytes. Curr Opin Immunol 2008;20:250-8.

23. Saijo K, Glass CK. Microglial cell origin and phenotypes in health and disease. Nat Rev Immunol 2011;11:775-87.

24. Nimmerjahn A, Kirchhoff F, Helmchen F. Resting microglial cells are highly dynamic surveillants of brain parenchyma in vivo. Science 2005;308:1314-8.

25. Glass CK, Saijo K, Winner B, Marchetto MC, Gage FH. Mechanisms underlying inflammation in neurodegeneration. Cell 2010;140:918-34.

26. Ransohoff RM, Cardona AE. The myeloid cells of the central nervous system parenchyma. Nature 2010;468:253-62.

27. Toescu EC, Moller T, Kettenmann H, Verkhratsky A. Long-term activation of capacitative Ca2+ entry in mouse microglial cells. Neuroscience 1998;86:925-35.

28. Hoffmann A, Kann O, Ohlemeyer C, Hanisch UK, Kettenmann H. Elevation of basal intracellular calcium as a central element in the activation of brain macrophages (microglia): suppression of receptor-evoked calcium signaling and control of release function. J Neurosci 2003;23:4410-9.

29. Farber K, Kettenmann H. Functional role of calcium signals for microglial function. Glia 2006;54:656-65.

30. O'Neill LA, Bowie AG. The family of five: TIR-domain-containing adaptors in Toll-like receptor signalling. Nat Rev Immunol 2007;7:353-64.

31. Neumann H, Kotter MR, Franklin RJ. Debris clearance by microglia: an essential link between degeneration and regeneration. Brain 2009;132:288-95.

32. Nagamoto-Combs K, Combs CK. Microglial phenotype is regulated by activity of the transcription factor, NFAT (nuclear factor of activated T cells). J Neurosci 2010;30:9641-6.

33. Koizumi S, Shigemoto-Mogami Y, Nasu-Tada K, Shinozaki Y, Ohsawa K, Tsuda M, et al. UDP acting at P2Y6 receptors is a mediator of microglial phagocytosis. Nature 2007;446:1091-5.

34. Nunes P, Cornut D, Bochet V, Hasler U, Oh-Hora M, Waldburger JM, et al. STIM1 juxtaposes ER to phagosomes, generating Ca(2)(+) hotspots that boost phagocytosis. Curr Biol 2012;22:1990-7.

35. Barcia C, Ros CM, Annese V, Carrillo-de Sauvage MA, Ros-Bernal F, Gomez A, et al. ROCK/Cdc42-mediated microglial motility and gliapse formation lead to phagocytosis of degenerating dopaminergic neurons in vivo. Sci Rep 2012;2:809.

36. Tsai FC, Seki A, Yang HW, Hayer A, Carrasco S, Malmersjo S, et al. A polarized Ca2+, diacylglycerol and STIM1 signalling system regulates directed cell migration. Nat Cell Biol 2014;16:133-44.

37. Neher E. Vesicle pools and Ca2+ microdomains: new tools for understanding their roles in neurotransmitter release. Neuron 1998;20:389-99.

38. Rizzuto R, Pozzan T. Microdomains of intracellular Ca2+: molecular determinants and functional consequences. Physiol Rev 2006;86:369-408.

39. Parekh AB. Ca2+ microdomains near plasma membrane Ca2+ channels: impact on cell function. J Physiol 2008;586:3043-54.

40. Lewis RS. The molecular choreography of a store-operated calcium channel. Nature 2007;446:284-7.

41. Quintana A, Pasche M, Junker C, Al-Ansary D, Rieger H, Kummerow C, et al. Calcium microdomains at the immunological synapse: how ORAI channels, mitochondria and calcium pumps generate local calcium signals for efficient T-cell activation. Embo j 2011;30:3895-912.

42. Demaurex N, Poburko D, Frieden M. Regulation of plasma membrane calcium fluxes by mitochondria. Biochim Biophys Acta 2009;1787:1383-94.

43. Henke N, Albrecht P, Pfeiffer A, Toutzaris D, Zanger K, Methner A. Stromal interaction molecule 1 (STIM1) is involved in the regulation of mitochondrial shape and bioenergetics and plays a role in oxidative stress. J Biol Chem 2012;287:42042-52.

44. Singaravelu K, Nelson C, Bakowski D, de Brito OM, Ng SW, Di Capite J, et al. Mitofusin 2 regulates STIM1 migration from the Ca2+ store to the plasma membrane in cells with depolarized mitochondria. J Biol Chem 2011;286:12189-201.

45. Tamashiro TT, Dalgard CL, Byrnes KR. Primary microglia isolation from mixed glial cell cultures of neonatal rat brain tissue. J Vis Exp 2012; doi:10.3791/3814.e3814.

46. Saura J, Tusell JM, Serratosa J. High-yield isolation of murine microglia by mild trypsinization. Glia 2003;44:183-9.

47. Chung WY, Park HW, Han JW, Lee MG, Kim JY. WNK4 inhibits plasma membrane targeting of NCC through regulation of syntaxin13 SNARE formation. Cell Signal 2013;25:2469-77.

48.   Honda S, Sasaki Y, Ohsawa K, Imai Y, Nakamura Y, Inoue K, et al. Extracellular ATP or ADP induce chemotaxis of cultured microglia through Gi/o-coupled P2Y receptors. J Neurosci 2001;21:1975-82.

49.   Ohsawa K, Irino Y, Nakamura Y, Akazawa C, Inoue K, Kohsaka S. Involvement of P2X4 and P2Y12 receptors in ATP-induced microglial chemotaxis. Glia 2007;55:604-16.

50.   Myrtek D, Idzko M. Chemotactic activity of extracellular nucleotideson human immune cells. Purinergic Signal 2007;3:5-11.

51.   Mosher KI, Andres RH, Fukuhara T, Bieri G, Hasegawa-Moriyama M, He Y, et al. Neural progenitor cells regulate microglia functions and activity. Nat Neurosci 2012;15:1485-7.

52.   Yokomizo T, Izumi T, Chang K, Takuwa Y, Shimizu T. A G-protein-coupled receptor for leukotriene B4 that mediates chemotaxis. Nature 1997;387:620-4.

53.   Davidson S, Truong H, Nakagawa Y, Giesler GJ, Jr. A microinjection technique for targeting regions of embryonic and neonatal mouse brain in vivo. Brain Res 2010;1307:43-52.

54.   Neher JJ, Neniskyte U, Hornik T, Brown GC. Inhibition of UDP/P2Y6 purinergic signaling prevents phagocytosis of viable neurons by activated microglia in vitro and in vivo. Glia 2014;62:1463-75.

55.   Domercq M, Vazquez-Villoldo N, Matute C. Neurotransmitter signaling in the pathophysiology of microglia. Front Cell Neurosci 2013;7:49.

56.   Kim B, Jeong HK, Kim JH, Lee SY, Jou I, Joe EH. Uridine 5'-diphosphate induces chemokine expression in microglia and astrocytes through activation of the P2Y6 receptor. J Immunol 2011;186:3701-9.

57.   Fang KM, Yang CS, Sun SH, Tzeng SF. Microglial phagocytosis attenuated by short-term exposure to exogenous ATP through P2X receptor action. J Neurochem 2009;111:1225-37.

58.   Bulavina L, Szulzewsky F, Rocha A, Krabbe G, Robson SC, Matyash V, et al. NTPDase1 activity attenuates microglial phagocytosis. Purinergic Signal 2013;9:199-205.

59.   Eichhoff G, Brawek B, Garaschuk O. Microglial calcium signal acts as a rapid sensor of single neuron damage in vivo. Biochim Biophys Acta 2011;1813:1014-24.

60. Davalos D, Grutzendler J, Yang G, Kim JV, Zuo Y, Jung S, et al. ATP mediates rapid microglial response to local brain injury in vivo. Nat Neurosci 2005;8:752-8.

61. Shah D, Romero F, Stafstrom W, Duong M, Summer R. Extracellular ATP mediates the late phase of neutrophil recruitment to the lung in murine models of acute lung injury. Am J Physiol Lung Cell Mol Physiol 2014;306:L152-61.

62. Perry VH, Nicoll JA, Holmes C. Microglia in neurodegenerative disease. Nat Rev Neurol 2010;6:193-201.

63. Yang S, Zhang JJ, Huang XY. Orai1 and STIM1 are critical for breast tumor cell migration and metastasis. Cancer Cell 2009;15:124-34.

64. Wei C, Wang X, Chen M, Ouyang K, Song LS, Cheng H. Calcium flickers steer cell migration. Nature 2009;457:901-5.

65. Lohmann C, Finski A, Bonhoeffer T. Local calcium transients regulate the spontaneous motility of dendritic filopodia. Nat Neurosci 2005;8:305-12.

66. Siddiqui TA, Lively S, Vincent C, Schlichter LC. Regulation of podosome formation, microglial migration and invasion by Ca(2+)-signaling molecules expressed in podosomes. J Neuroinflammation 2012;9:250.

67. Becherer U, Moser T, Stuhmer W, Oheim M. Calcium regulates exocytosis at the level of single vesicles. Nat Neurosci 2003;6:846-53.

68. Zenisek D, Davila V, Wan L, Almers W. Imaging calcium entry sites and ribbon structures in two presynaptic cells. J Neurosci 2003;23:2538-48.

ABSTRACT (in Korean)

미세아교세포에서 STIM1 에 의해 매개되는
칼슘신호 전달기전을 통한 면역기능의 조절

<지도교수 김 주 영>

연세대학교 대학원 의과학과

임 혜 민

진핵세포에서 칼슘이온의 조절은 세포의 삶과 죽음을 결정지을 수 있는 중요한 세포 내 신호전달물질이기 때문에 이에 대한 연구가 중요하다. 활성화된 면역세포의 분화에는 항원 자극 이후 지속적으로 높은 농도의 세포질 내 칼슘이 면역세포의 증식, 사이토카인 분비, 식세포 작용 등 매우 중요하다고 알려져 있다. 다양한 종류의 면역세포들을 이용하여 SOCE 를 통한 칼슘 유입이 미치는 면역세포의 기능에 대한 연구가 활발히 진행되는 추세이지만, 면역세포마다 SOCE 가 미치는 영향력이 조금씩 다르기 때문에 각 면역세포에서의 정확한 이해가 필요한 실정이다. STIM1 은 세포 내 칼슘 저장고인 소포체에서 칼슘 결핍 신호에 의해 세포막의 ORAI1 과 기능적 단위를 이루어 SOCE (Store-Operated Ca^{2+} Entry) 를 통해서 세포 밖의 칼슘을 세포질 내로 유입시키는 SOC 의 구성 단백이다. 세포질 내로 유입된 칼슘은 칼슘농도 의존적 인산화·탈인산화 단백 및 NFAT 을 비롯한 다양한 칼슘의존적 전산인자들을 통해 유전자 발현의 변화, 세포 성장과 같은 long-term cellular response 에 필요한 칼슘신호를 유발하는데 매우 중요한 역할을 한다. 한편, 세포막 수용체 자극으로 국소적으로 발생한 칼슘신호는 신속하게 국소적 탈부착 및 변형과 관련된 골격단백들 및 인산화단백의 조절을 위해서 필요하며, 세포의 신속한 이동이나 식세포작용에 중요한 것으로 알려져 있다.

본 연구에서는 RIKEN 의 Kurosaki 연구진으로부터 분양 받은 C57BL/6 계통의 *Stim1* 유전자가 소실된 마우스를 이용하였다. *Stim1* 소실은 근병증을 유도하여 출산 직후, 치사(致死)하므로 17일 경의 배아의 뇌를 일차배양 하여 얻은 미세아교세포를 실험에 적용하였다. LPS 처리에 의해 활성화 된 정상 미세아교세포는 감염원을 제거하기 위해 Pro-inflammatory 인자들을 분비하게 되는데, *Stim1* 소실 미세아교 세포에서는 TNF-α와 IL-6 의 사이토카인 분비 감소, 식세포 작용의 저하 및 single live cell $[Ca^{2+}]_i$ imaging 기법을 이용하여 SOCE 를 통한 칼슘 유입이 거의 이루어지지 않음을 확인하였다. 또한, FACS 를 이용한 UDP 에 의한 식세포 작용 및 *in vitro* 상에서 chemotaxis chamber 를 이용한 ATP 에 의한 세포이동 능력이 저하 되어 있음을 확인하였다. 교배시킨 *Stim1* 소실 hetero 암컷 마우스를 호흡 마취 시켜 배아의 한쪽 뇌에 LPS 를 microinjection 한 뒤, 24시간 후에 정상 및 *Stim1* 소실 배아의 뇌 조직에 활성화 된 미세아교세포의 몰려든 수를 비교한 결과, *in vivo* 상에서도 세포이동 능력은 저하 되었다. 위의 본 연구 결과들을 통해서, 미세아교세포에서 STIM1 단백에 의해 매개되는 칼슘신호 전달기전을 통해 면역기능이 조절된다는 사실을 확인하였다.

한편, STIM1 과 ORAI1 의 분자적 메커니즘을 살펴보고자, TG, UDP, LPS 등 자극을 준 뒤, 세포 표면에 발현하는 ORAI1 의 움직임을 면역염색법을 통해 관찰하였다. TG 처리시, *Stim1* 소실 미세아교세포에서도 cell periphery 끝부분까지 세포막 ORAI1 발현이 약간 증가했지만, 세포 밖의 칼슘을 유입시키는 기능적 단위를 이루기 위해서는 반드시 STIM1 이 필요하다는 사실을 정상 미세아교세포의 확장된 ORAI1 의 cluster size 를 통해 확인했다. 또한, UDP 자극에 따른 세포막 ORAI1 이 cell periphery 에 발현하거나, 혹은 LPS 처리에 의해 핵 주변부에 발현하기 위해서는 모두 STIM1 이 필요하다는 사실을 확인 하였다.

이동하는 세포의 periphery 에는 'calcium flicker' 라고 불리는 고농도의 칼슘이 micro-domains 에 국소적으로 존재하다 사라지는 이 부위로 인해서 세포가 방향성 있게 움직이는 등 periphery 의 국소적 칼슘신호와 세포 움직임의 연관성이 보고 된 바 있다. 세포 이동 능력이 저하되어 있는 *Stim1* 소실 미세아교세포의 peripheral 부위에서 칼슘신호의 변동 정도를 확인한 결과, 뜻밖에도, *Stim1* 소실 군에서 cell periphery 에서 칼슘농도의 변동이 매우 큰 현상이 관찰되었고, 그 cell periphery 의 국소적 부위와 단일세포 전체의 칼슘 움직임과는 무관함을 발견하였다. 이러한 국소적 칼슘농도변화 (이하 칼슘요동)의 원인을 규명하기

위하여 세포 밖 칼슘농도가 없는 조건에서 관찰한 결과, 칼슘요동은 폭이 약간 감소하였지만 여전히 일어났다. 또한 2-APB 처리로 소포체의 IP$_3$R 를 차단하였을 때는 칼슘요동현상이 억제되지 않은 반면, CCCP 나 Rotenone 을 각각 처리하여 미토콘드리아의 막전위를 억제하면, 칼슘요동현상이 억제되는 것이 확인되었다. 위의 결과를 통해서 STIM1 의 부재 시, 미토콘드리아의 Ca^{2+} micro-domains 의 칼슘농도 조절능력에 결핍이 발생하는 것을 확인하였다. 또한, cell periphery 에서의 칼슘요동현상이 미처 이동하지 못한 세포막 ORAI1 이 기여하는지를 확인하고자, Extracellular-Orai1 항체 및 SKF-96365 약물을 이용하여 SOC 를 봉쇄하였고, 칼슘요동현상이 저해되는 것이 모두 확인 되었다. 반면, SACC 채널의 억제제인 Streptomycin 을 처리 하였을 때는 저해되지 않았다. 이러한 현상은 미토콘드리아의 국소적 칼슘농도조절에 SOCE 를 통한 칼슘유입에 영향을 받는다는 알려진 사실과 연관하여 볼 때, STIM1 부재 시 나타나는 칼슘요동이 미토콘드리아의 국소적 칼슘농도 조절능력의 결함에 의한 결과임을 다시 한번 확인시켜 주었다.

결론적으로 본 연구는 미세아교세포의 면역반응을 매개하는 칼슘신호에 전반적으로 STIM1 이 관련되어 있음을 규명하였다. 그 중 특히 신속한 움직임과 연관된 국소적 칼슘신호조절에 STIM1 이 매우 중요한 조절자임을 규명하였으며, 그 관련기전으로 세포 내 국소적 칼슘농도를 조절하고 있는 미토콘드리아의 칼슘유·출입능이 STIM1 에 의해 조절됨을 최초로 제안하는 바이다.

핵심되는 말: STIM1, SOCE, 칼슘 유입, 미세아교세포, 면역기능, 식세포 작용, 세포 이동, 국소적인 칼슘 움직임, 칼슘요동현상, 미토콘드리아

PUBLICATION LIST

1. Heo DK*, **<u>Lim HM</u>***, Nam JH, Lee MG, Kim JY. Regulation of phagocytosis and cytokine secretion by store-operated calcium entry in primary isolated murine microglia. Cellular signalling. 2015 Jan;27(1):177-86.   **(* equal contribution)**

2. Ahn HK*, Kang YW*, **<u>Lim HM</u>***, Hwang I, Pai HS. Physiological Functions of the COPI Complex in Higher Plants. Molecules and cells. 2015 Oct 2. doi: 10.14348/molcells.2015.0115. [Epub ahead of print].   **(* equal contribution)**